

Sampling as Bandits: Evaluation-Efficient Design for Black-Box Densities

Takuo Matsubara^{1*} Andrew Duncan² Simon Cotter³ Konstantinos Zygalakis¹

¹The University of Edinburgh ²Imperial College London ³The University of Manchester

Abstract

We introduce bandit importance sampling (BIS), a new class of importance sampling methods designed for settings where the target density is expensive to evaluate. In contrast to adaptive importance sampling, which optimises a proposal distribution, BIS directly designs the samples through a sequential strategy that combines space-filling designs with multi-armed bandits. Our method leverages Gaussian process surrogates to guide sample selection, enabling efficient exploration of the parameter space with minimal target evaluations. We establish theoretical guarantees on convergence and demonstrate the effectiveness of the method across a broad range of sampling tasks. BIS delivers accurate approximations with fewer target evaluations, outperforming competing approaches across multimodal, heavy-tailed distributions, and real-world applications to Bayesian inference of computationally expensive models.

1 Introduction

Recent advances in machine learning and data science have broadened the scope of statistical analysis to encompass highly complex phenomena (Chen et al., 2010). The precise statistical description of complex phenomena often relies on highly-structured, black-box models that are computationally expensive to evaluate. Bayesian inference offers coherent probabilistic reasoning for deducing appropriate models from observations and prior knowledge. Yet, Bayesian inference can be computationally impractical for black-box models. Many cases emerge in, e.g., computational physics, biology, and geostatistics, where the model likelihoods depend on dynamical equations that need to be numerically solved (Beaumont et al., 2002; Girolami, 2008; Marin et al., 2012; Warne et al., 2020) or components involving exceedingly-large matrices and summations (Rue and Held, 2005; Goodreau et al., 2009; Besag, 1986).

The chief concern in Bayesian inference is to sample from a posterior density of the model parameter, proportional to the model likelihood and a prior density. By design, standard sampling methods, such as Markov-Chain Monte Carlo (MCMC; Brooks et al., 2011), require a large number of evaluations of the target density for different parameter values. The computational cost quickly exceeds a desirable budget if the target density is expensive to evaluate. Thus, from a practical viewpoint, there is a need for novel sampling methods designed for black-box densities, which require only a small number of target evaluations.

*The corresponding author’s email address: takuo.matsubara@ed.ac.uk

Importance sampling—originally introduced as a variance reduction technique in Monte Carlo estimation (Hammersley and Morton, 1954)—is an appealing approach in this context. The target density is approximated by a weighted average of samples drawn from an arbitrary proposal density (Tokdar and Kass, 2010). Given samples from the proposal density, evaluations of the target density occur only up to the number of the samples. However, the design of the samples is a determinant factor in the approximation accuracy of importance sampling. Adaptive importance sampling (AIS) is arguably the most common approach to the effective design of the samples, which optimises the proposal density so that it approximates the target density (e.g. Bugallo et al., 2017; Cotter et al., 2019, 2020). Yet, AIS can be easily impractical for black-box densities, as it reintroduces the need for intensive evaluation of the target density to optimise the proposal density.

In machine learning, Bayesian optimisation (BO; Mockus, 1989) has gained immense attention for problems involving black-box objective functions that are expensive to evaluate (Shahriari et al., 2016). The key idea is to replace the black-box objective with a computationally-cheap surrogate model constructed from the record of objective values evaluated in the past. Gaussian process (GP; Rasmussen and Williams, 2005) is a particularly successful choice in surrogate modelling (Gramacy, 2020). It not only provides predictions based on interpolation of the observed values, but also estimates the uncertainty in them arising from the non-identifiability of the true function given a finite amount of data. BO iteratively selects points that maximise a specified acquisition criterion based on the GP surrogate model. BO—sometimes referred to as GP bandits—can be viewed as a bandit problem with infinitely many arms (Bull, 2011). Hence, the framework of BO has been leveraged for experimental designs and active learning problems (Srinivas et al., 2010).

Contribution This work establishes bandit importance sampling (BIS), a novel class of importance sampling that provides adaptively-designed samples. BIS retains the original advantage of importance sampling in that the target density is evaluated only up to the number of samples. It drastically reduces the number of samples compared to the level that standard MCMC or importance sampling typically requires for accurate approximation of the target density. The approach of BIS is to combine importance sampling with multi-armed bandits. AIS optimises the proposal density and draws samples randomly. In contrast, BIS optimises over the samples directly, sequentially selecting them from a pool of candidates based on a bandit strategy. The bandit strategy of BIS capitalises on GP surrogate modelling of the target density. While experimental designs for GPs aim to recover a target function with GPs in general, BIS recovers the target density with the design points guided by the GP bandits. We establish convergence guarantees for the weighted samples of BIS, independently of the convergence of the GP surrogate model itself.

Space-filling sequences—such as the Halton sequence (Halton, 1964)—can serve well as the candidate pool used in BIS, from which the samples are selected. It is a celebrated result in quasi-Monte Carlo (QMC; Dick and Pillichshammer, 2010) that numerical integration based on N points from a space-filling sequence achieves the convergence rate $\mathcal{O}((\log N)^{d-1}N^{-1})$. This is faster than the concentration rate of Monte Carlo integration, $\mathcal{O}(N^{-1/2})$, for a large sample size N (Morokoff and Caflisch, 1994). Yet, importance sampling with the space-filling sequence can be inefficient for small to medium sample sizes N . This is because space-filling sequences are not adaptive to the high-probability region of the target density, as they are designed to explore the domain uniformly. Using a space-filling sequence in BIS corresponds to changing the order of the space-filling sequence so that the high-probability region of the target density is explored first. This allows for efficient approximation accuracy for both small and large sample sizes N .

Structure The rest of the paper is structured as follows. Section 2 concisely recaps importance sampling and GP regression. Section 3 introduces the methodology of BIS in full. Section 4 establishes a theoretical analysis of the rate of the convergence. Section 5 examines the empirical performance of BIS, with applications to Bayesian inference of computationally-expensive models. Relevant work on GP-based experimental designs for Bayesian computation is recapped in Section 6. Finally, Section 7 concludes the paper with a discussion of future directions.

2 Background

This section provides a concise overview of importance sampling and GP regression. Let $\Theta \subset \mathbb{R}^d$ for some dimension d . Any probability distribution on Θ considered in this work is a Borel probability distribution and identified with the density with respect to the Lebesgue measure if it exists.

2.1 Importance Sampling

Importance sampling is one of the most fundamental sampling methods, which is suitable when drawing samples from a density of interest $p(\theta) = q(\theta)/Z$ on Θ is undesirable. The aim is to produce a set of M weighted samples, $\{\theta_n, w_n\}_{n=1}^M$, which approximates the density $p(\theta)$. The samples $\{\theta_n\}_{n=1}^M$ are drawn from a proposal density $u(\theta)$ in lieu of $p(\theta)$. If the density $p(\theta)$ is known in full, the weights $\{w_n\}_{n=1}^M$ are each set to the ratio $p(\theta_n)/u(\theta_n)$. If the density $p(\theta)$ is known only up to the normalisation constant Z , the *self-normalised* weights $\{w_n\}_{n=1}^M$ are used, where the expectation of an integrand $f(\theta)$ with respect to $p(\theta)$ is estimated as

$$\mathbb{E}_{\theta \sim p}[f(\theta)] \approx \sum_{i=1}^M w_i f(\theta_i) \quad \text{where} \quad w_n = \frac{q(\theta_n)/u(\theta_n)}{\sum_{n=1}^M q(\theta_n)/u(\theta_n)}.$$

The weights depend on the proportional $q(\theta)$ only, as the self-normalisation cancels out the constant Z . Consistency of the Monte Carlo estimate above is well established.

For importance sampling to be efficient, a sufficient portion of the samples $\{\theta_n\}_{n=1}^M$ should be situated well around the high-probability region of the target density $p(\theta)$. Otherwise, samples with insignificant weights near zero will be dominant, resulting in little contribution to the approximation of the density $p(\theta)$. The panel (a) in Figure 1 illustrates a case where only around 10% of samples have significant weights while the other 90% are negligible. AIS improves the efficiency of importance sampling by optimising the proposal density $u(\theta)$ to draw samples. In AIS, a parametric family of proposal densities is typically specified, and samples are drawn from the family after or along the optimisation process. This approach is, however, not ideal for our setting, as successful optimisation of the proposal density $u(\theta)$ requires intensive evaluations of the target density $p(\theta)$. On top of that, as the samples are random and independent, some can be redundant, failing to be the most informative point to evaluate the target density $p(\theta)$.

Suppose that the density $p(\theta)$ is so computationally expensive that the proportional $q(\theta)$ can be evaluated only up to N times. A natural desideratum under such circumstances is to find N samples that lead to the most accurate approximation of the density $p(\theta)$ via importance sampling. In the panel (a) in Figure 1, for example, where 200 samples are drawn, selecting N samples among them with the largest weights achieves the best accuracy under N density evaluations. To this end, we cast sampling as a bandit problem to sequentially select N most effective points from a pool of M well-dispersed points that can be easily drawn. See the panel (b) in Figure 1 for illustration.

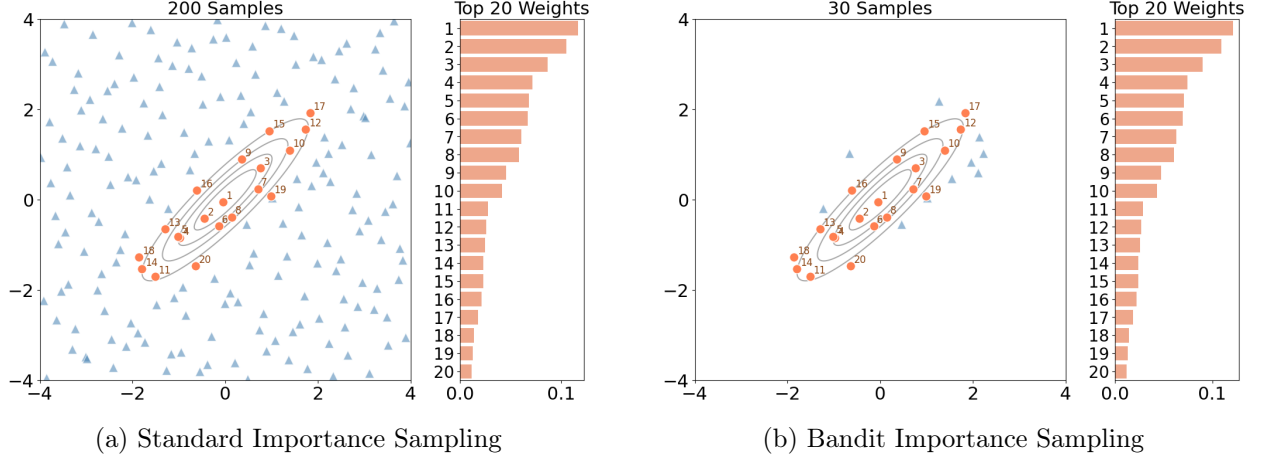


Figure 1: Illustration of two sampling schemes (a) and (b) applied to a normal density (solid line). The left panel shows 200 quasi-uniform points used as samples, where the points associated with the top 10% weights are circular, and the rest are triangular. The right panel shows 30 samples selected by BIS from the same 200 quasi-uniform points, where BIS exhausted all the points with the top 10% weights within 30 density evaluations.

2.2 GP Regression

A GP, denoted by $\mathcal{GP}(m, k)$, is a stochastic process determined by a mean function $m : \Theta \rightarrow \mathbb{R}$ and a covariance kernel $k : \Theta \times \Theta \rightarrow \mathbb{R}$. It can be understood as a random variable $f \sim \mathcal{GP}(m, k)$ taking values in a space of functions on Θ . A characteristic property of GPs is the moment conditions

$$m(\theta) = \mathbb{E}_{f \sim \mathcal{GP}(m, k)}[f(\theta)] \quad \text{and} \quad k(\theta, \theta') = \mathbb{E}_{f \sim \mathcal{GP}(m, k)}[(f(\theta) - m(\theta))(f(\theta') - m(\theta'))],$$

which hold pointwise. Another characteristic property of GPs is that the joint law of the image $(f(\theta_1), \dots, f(\theta_n))$ of inputs $(\theta_1, \dots, \theta_n)$, under the sample path $f \sim \mathcal{GP}(m, k)$, follows a multivariate Gaussian distribution $\mathcal{N}(\mathbf{m}_n, \mathbf{K}_n)$. Here the mean $\mathbf{m}_n \in \mathbb{R}^n$ is a vector whose i -th element is $m(\theta_i)$ and the covariance $\mathbf{K}_n \in \mathbb{R}^{n \times n}$ is a matrix whose (i, j) -th element is $k(\theta_i, \theta_j)$. Common choices of the covariance kernel k include Gaussian and Matérn kernels. See e.g. Rasmussen and Williams (2005) for a more detailed introduction to GPs.

GPs provide a framework for nonparametric Bayesian modelling of regression problems. Suppose that a set of inputs $(\theta_1, \dots, \theta_n)$ and the associated outputs (y_1, \dots, y_n) are observed as data. Given a GP prior distribution $\mathcal{GP}(m, k)$ and the observed data $(\theta_i, y_i)_{i=1}^n$, the posterior distribution remains as a GP, denoted by $\mathcal{GP}(m_n, k_n)$, where the mean function m_n and covariance kernel k_n are updated from those of the GP prior as follows:

$$m_n(\theta) = \mathbf{k}_n(\theta)^T \mathbf{K}_n^{-1} (\mathbf{y}_n - \mathbf{m}_n),$$

$$k_n(\theta, \theta') = k(\theta, \theta') - \mathbf{k}_n(\theta)^T \mathbf{K}_n^{-1} \mathbf{k}_n(\theta').$$

Here, $\mathbf{k}_n(\theta)$ denotes a vector-valued function defined by $\mathbf{k}_n(\theta) = (k(\theta, \theta_1), \dots, k(\theta, \theta_n)) \in \mathbb{R}^n$, and $\mathbf{y}_n \in \mathbb{R}^n$ denotes a vector whose i -th element is y_i . In practice, it is common to assume that each output value is realised under i.i.d. observation noise $\epsilon \sim \mathcal{N}(0, \sigma^2)$, in which case \mathbf{K}_n is replaced with $\mathbf{K}_n + \sigma \mathbf{I}_{n \times n}$ —where $\mathbf{I}_{n \times n}$ is the $n \times n$ identity matrix—in the above definition.

3 Methodology

We now introduce BIS, a method that frames the design of adaptive samples as a bandit problem. Section 3.1 presents a general framework of BIS. It is built on two components: (i) a pool of candidates from which samples are selected; (ii) a criterion to select a sample at each iteration. Section 3.2 discusses our default choice of the candidate pool. Section 3.3 defines our point-selection criterion, termed GP upper Jensen bound (GP-UJB), which capitalises on a GP surrogate density. Section 3.4 provides a discussion of the choice of hyperparameters involved in GP-UJB.

Setup: Suppose $\Theta \subset \mathbb{R}^d$ is a compact hyperrectangular domain with no loss of generality, since reparametrisation can be performed otherwise. Let $p(\theta) = q(\theta)/Z$ be a target density of interest on Θ , where $q(\theta)$ denotes the proportional term and Z denotes the normalisation constant. Assume that $p(\theta)$ is positive over Θ . A practical scenario in mind is that evaluation of the proportional $q(\theta)$ is possible at each θ but computationally expensive for one’s computational capacity.

3.1 Bandit Importance Sampling

The aim of BIS is to produce a set of N weighted samples, $\{\theta_n^*, w_n^*\}_{n=1}^N$, which approximates the target density $p(\theta)$, requiring only N evaluations of the proportional $q(\theta)$ in total. Rather than drawing samples randomly from a proposal distribution, BIS directly optimises the samples themselves. BIS selects each sample sequentially from a pool of candidates under a chosen criterion. This can be viewed as a multi-armed bandit problem, where at each iteration a new sample is selected based on current information. Notably, once a point is selected in BIS, it is not revisited in future iterations (see Remark 1), distinguishing it from conventional bandit formulations.

We detail the iterative procedure of BIS. Let $u(\theta)$ be a proposal density on Θ . Let $\mathcal{U} = \{\theta_i\}_{i=1}^\infty$ be a sequence that weakly converges to $u(\theta)$, which we call a *proposal sequence*. Let S_n denote a pool of candidates at each iteration n . At the first iteration $n = 1$, we use the first M points of the proposal sequence \mathcal{U} as the selection pool $S_1 = \{\theta_i\}_{i=1}^M$. The candidate pool S_n is updated after each iteration, replacing the selected point with a new point from the proposal sequence. This assures no point in the proposal sequence \mathcal{U} will be selected twice. Finally, let $U_n(\theta)$ be a point-selection criterion specified at each iteration n . We repeat the following steps from $n = 1$:

1. choose a point θ_n^* in the candidate pool S_n , which maximises the criterion $U_n(\theta)$;
2. evaluate the target proportional $q(\theta_n^*)$ for evaluation of the importance weight w_n^* ;
3. specify the candidate pool S_{n+1} at the next iteration by $S_{n+1} = (S_n \setminus \{\theta_n^*\}) \cup \{\theta_{M+n}\}$.

We assign the self-normalised weight $w_n^* = (q(\theta_n^*)/u(\theta_n^*)) / \sum_{i=1}^N (q(\theta_i^*)/u(\theta_i^*))$ to each of the samples $\{\theta_n^*\}_{n=1}^N$ after the last iteration N . Note that the size of the candidate pool, $|S_n|$, is constant at $|S_n| = M$ across all iterations. Algorithm 1 summarises the explicit procedure.

Remark 1 (Importance of Discrete Optimisation with No Revisit). BIS selects a point by optimisation of the criterion U_n over the discrete set S_n , under the constraint that points selected in the past will never be revisited. A possible alternative, similarly to BO, is to select a point by optimisation of the criterion U_n over the continuous set Θ . However, as we shall demonstrate in Appendix C.1, the latter approach can situate an excessive portion of samples around the mode of the target density. Consequently, this derails the convergence of the resulting weighted samples, in addition to causing

Algorithm 1: Bandit Importance Sampling

Input: sample size N , candidate-pool size M , proposal sequence $\{\theta_i\}_{i=1}^{M+N}$ convergent to proposal density u , point-selection criterion U_n for each iteration n

Output: weighted samples $\{\theta_n^*, w_n^*\}_{n=1}^N$ to approximate the target density p

$S_1 \leftarrow \{\theta_i\}_{i=1}^M$ ▷ initialise selection pool

for $n \leftarrow 1, \dots, N$ **do**

$\theta_n^* \leftarrow \arg \max_{\theta \in S_n} U_n(\theta)$ ▷ optimise point-selection criterion

$w_n^* \leftarrow \frac{q(\theta_n^*)}{u(\theta_n^*)}$ ▷ evaluate density ratio $\frac{q(\cdot)}{u(\cdot)}$

$S_{n+1} \leftarrow (S_n \setminus \{\theta_n^*\}) \cup \{\theta_{M+n}\}$ ▷ update selection pool

end

$(w_1^*, \dots, w_N^*) \leftarrow (w_1^*, \dots, w_N^*) / \sum_{n=1}^N w_n^*$ ▷ normalise weights

redundant density evaluations around the mode. On the other hand, the use of the discrete set S_n in BIS serves as a regularisation to prevent overconcentration of the selected points. In combination with that, the mechanism of not revisiting the past points ensures the convergence of the samples to the target posterior (c.f. Section 4).

3.2 Proposal Density and Proposal Sequence

We discuss a choice of the proposal density u and the proposal sequence $\mathcal{U} = \{\theta_i\}_{i=1}^\infty$ in BIS. In standard importance sampling, there exists an optimal proposal density in terms with the variance reduction of the Monte Carlo estimation. However, such a proposal density depends on the target density itself, which is black-box and not available in our setting. In the first place, the lack of information on the target density—such as the mode and the decay of the tail probability—means that we have little knowledge with which to design the proposal density. We therefore consider the uniform density over the domain Θ as a natural default choice of the proposal density u .

Note that the proposal sequence \mathcal{U} does not have to be i.i.d. random samples from the proposal density u , since unbiasedness is no longer of interest in BIS. Any dependent random sequence or deterministic sequence can be used if it converges to u . In this regard, space-filling sequences in QMC exhibit fast convergence to the uniform proposal density u (Morokoff and Caflisch, 1994). Our default choice of the proposal sequence is the Halton sequence (Halton, 1964), which is arguably the most common space-filling sequence in practice. It is originally defined for the unit-cube domain but is immediately amenable to hyperrectangular domains. For clarity, we define a version of the Halton sequence scaled to the hyperrectangular domain $\Theta = [a_{(1)}, b_{(1)}] \times \dots \times [a_{(d)}, b_{(d)}]$, where $a_{(i)}$ and $b_{(i)}$ denote the left and right boundary of the domain at the i -th coordinate.

Definition 1 (Scaled Halton Sequence). *Given the Halton sequence $\{\eta_i\}_{i=1}^\infty$ on the unit cube $[0, 1]^d$, the scaled Halton sequence $\{\theta_i\}_{i=1}^\infty$ on the domain Θ is defined by $\theta_i := A + B\eta_i$, where $A := (a_{(1)}, \dots, a_{(d)}) \in \mathbb{R}^d$ and $B = \text{diag}(b_{(1)} - a_{(1)}, \dots, b_{(d)} - a_{(d)})$ is a $d \times d$ diagonal matrix.*

Using the Halton sequence in BIS is an effective approach to approximation of black-box densities. Regardless of sampling methods, tracking down the complete geometry of the black-box density necessitates the density to be evaluated everywhere in the domain Θ . The Halton sequences provide a sophisticated design of points that explores the entire domain. BIS then selects points around the high-probability region of the target density at the early iterations by the bandit strategy.

3.3 Point-Selection Criterion

The point-selection criterion U_n focused in this paper is built upon a GP surrogate model of the target density $p(\theta) = q(\theta)/Z$. Whereas densities take only positive values, GPs take both negative and positive values. A common strategy to fit a GP to the density is to apply the log-transformation to the value of the density. More generally, any other transformations that map positive values to \mathbb{R} can be used. This can be stated more formally as below.

Let $\phi : \mathbb{R} \rightarrow [0, \infty)$ be a convex non-negative function s.t. the inverse ϕ^{-1} exists at least for the positive range $(0, \infty)$. Then the proportional $q(\theta)$ of the target density can be expressed as $q(\theta) = \phi(\phi^{-1}(q(\theta)))$. We shall model the transformed term $\phi^{-1}(q(\theta))$ by a GP. For example, choosing the exponential map $\phi(\cdot) = \exp(\cdot)$ recovers the log-transformation $\phi^{-1}(\cdot) = \log(\cdot)$ as the inverse. Now, we introduce our point-selection criterion, GP-UJB, which is equipped with several appealing properties for multi-armed bandits.

Definition 2 (GP-UJB). *Given a GP posterior $\mathcal{GP}(m_n, k_n)$ conditional on a set of n evaluations $\{\theta_i, \phi^{-1}(q(\theta_i))\}_{i=1}^n$, GP-UJB is a function $U_n : \Theta \rightarrow \mathbb{R}$ defined pointwise by*

$$U_n(\theta) := \mathbb{E}_{f \sim \mathcal{GP}(m_n, k_n)} [\phi(f(\theta))]$$

where $f(\theta)$ denotes the value of the GP sample path $f \sim \mathcal{GP}(m_n, k_n)$ evaluated at θ .

Driving both exploitation and exploration is a pivotal factor in most bandit problems. GP-UJB gives an upper bound of the ‘least-error’ plug-in approximation $\phi(m_n(\theta))$ of the proportional $q(\theta)$ based on the GP posterior mean m_n . That is, we have $U_n(\theta) = \mathbb{E}_{f \sim \mathcal{GP}(m_n, k_n)} [\phi(f(\theta))] \geq \phi(m_n(\theta))$ as an immediate consequence of Jensen’s inequality. Therefore, GP-UJB admits the following decomposition into two terms that drive, respectively, exploitation and exploration:

$$U_n(\theta) = \underbrace{\phi(m_n(\theta))}_{\text{exploitation}} + \underbrace{\mathbb{E}_{f \sim \mathcal{GP}(m_n, k_n)} [\phi(f(\theta))] - \phi(m_n(\theta))}_{\text{exploration}}.$$

The first term corresponds to the least-error approximation of the proportional $q(\theta)$ achievable by the GP, hence driving exploitation of past information. The second term, known as the Jensen’s gap, is always non-negative due to Jensen’s inequality. It corresponds to the excess deviation between GP-UJB and the least-error GP approximation of the proportional. The second term amplifies according to the level of uncertainty in the GP posterior at each location θ , hence driving exploration of where the GP posterior is uncertain. The second term equals zero at the training points $\{\theta_i\}_{i=1}^n$, where the GP posterior has no uncertainty.

We can guarantee that the L2 error between GP-UJB and the target proportional $q(\theta)$ is controlled by the average-case interpolation error of the GP regression. Moreover, if an additional regularity condition is met, the former is specifically smaller than the later. This also supports the use of GP-UJB as it converges faster than the concentration of the GP posterior itself. In the following result, $\|\cdot\|_{L_2(\Theta)}$ denotes the L2 norm of functions on Θ under the Lebesgue measure.

Proposition 1. *Let $g(\theta) := \phi^{-1}(q(\theta))$, that is, $q(\theta) = \phi(g(\theta))$. Suppose that ϕ is differentiable in $(0, \infty)$ with the derivative ϕ' satisfying $|\phi'(a)| \leq \exp(a)$ for all $a \in (0, \infty)$. Let $U_n(\theta)$ be GP-UJB with the GP posterior $\mathcal{GP}(m_n, k_n)$. It holds for some constant $C > 0$ that*

$$\|U_n - q\|_{L_2(\Theta)}^2 \leq C \mathbb{E}_{f \sim \mathcal{GP}(m_n, k_n)} [\|f - g\|_{L_2(\Theta)}^2].$$

In particular, if $g(\theta) < -1/2$ and $m_n(\theta) + k_n(\theta, \theta) < -1/2$, we have $C < 1$.

Proof. The proof is provided in Appendix B.1. \square

Remark 2. Proposition 1 assures that, if the GP posterior converges, the GP-UJB also converges. Convergence analysis of the average-case GP regression error in the right-hand side is well established; see e.g. Kanagawa et al. (2018). The condition $g(\theta) < -1/2$ and $m_n(\theta) + k_n(\theta, \theta) < -1/2$, under which we have $C < 1$, is mild when $\phi^{-1} = \log$. We can take a constant $0 < B < 0.5$ and assume $q(\theta) \leq B$ without loss of generality, because otherwise we can redefine the proportional $q(\theta)$ by dividing it by some constant so that the condition hold, where the density $p(\theta)$ remains invariant due to normalisation. By the bound, the log-proportional satisfies $g(\theta) = \log q(\theta) \leq \log B < -1/2$. Since $m_n(\theta)$ is the GP posterior mean that approximates $g(\theta)$ and $k_n(\theta, \theta)$ is bounded, the latter condition $m_n(\theta) + k_n(\theta, \theta) < -1/2$ holds by taking the bound B small enough that $m_n(\theta) + k_n(\theta, \theta)$ does not exceed $-1/2$. Regardless, the latter condition is easy to verify numerically.

3.4 Hyperparameters of GP-UJB

Finally, we discuss the default setting of the hyperparameters of GP-UJB. The first hyperparameter of GP-UJB is the convex non-negative function ϕ . The second hyperparameter of GP-UJB is a hyperparameter of the mean and covariance functions of the GP prior.

The balance between exploitation and exploration driven by GP-UJB is automatically adjusted by the choice of ϕ . Choosing the function ϕ that results in a closed-form expression of GP-UJB is computationally appealing. Examples of closed-form GP-UJBs are summarised in Table 1. Modelling the log-proportional $\log q(\theta)$ by GPs has been proven to be successful in multiple applications (e.g. Osborne et al., 2012; Järvenpää et al., 2021). Following these work, we suggest the exponential map $\phi(\cdot) = \exp(\cdot)$ as the default choice, which recovers the log-transformation $\phi^{-1}(\cdot) = \log(\cdot)$ as the inverse. This default choice is also supported by Remark 2. Simulation studies on other choices of ϕ are provided in Appendix C.2.

Table 1: Examples of closed-form expressions of GP-UJB for different functions ϕ , where we denote by φ and Φ the probability density function and the cumulative distribution function of the standard normal distribution, respectively, and let $\sigma_n(\theta) := \sqrt{k_n(\theta, \theta)}$ for better presentation.

function $\phi(x)$	inverse $\phi^{-1}(x)$	GP-UJB $U_n(\theta)$
$\exp(x)$	$\log(x)$	$\exp(m_n(\theta) + 0.5\sigma_n^2(\theta))$
$\max(0, x)$	x	$m_n(\theta)\varphi(m_n(\theta)/\sigma_n(\theta)) + \sigma_n(\theta)\Phi(m_n(\theta)/\sigma_n(\theta))$
x^2	\sqrt{x}	$m_n^2(\theta) + \sigma_n^2(\theta)$

Equipping the mean and covariance function of a GP prior with some hyperparameter ψ is a common practice in GP regression. Finding an appropriate value of the hyperparameter ψ maximises the performance of GP regression in general. Common examples of the hyperparameter ψ include the length and variance constant of the Gaussian or Matérn covariance kernel. Typically, the hyperparameter ψ is selected by maximising the log-likelihood of the GP posterior. For BO, using the maximum likelihood estimate of ψ at each iteration is vital for a successful outcome. Following this standard practice, we use the maximum likelihood estimate of the hyperparameter ψ for GP-UJB at each iteration.

Remark 3 (Initial Points). In sequential experimental designs for GPs, GP surrogate models at the first few iterations can be a poor approximation of a function of interest. This is because

GPs can overfit to a very small number of data points. Selecting the first few points at random, without optimisation, is a widely-used strategy to improve stability of the GP surrogate model at early iterations. Algorithm 1 of BIS is immediately amenable for the same strategy, where for some integer $N_0 > 0$ the first N_0 points $\{\theta_n^*\}_{n=1}^{N_0}$ of the samples can be set to the first N_0 points of the scaled Halton sequence without optimisation.

Remark 4 (Limitations). In this work, we limit our focus to densities in low-dimensional domains. Difficulties in both scalability and accuracy of GPs in high dimensions is a well-recognised open challenge. Besides, sampling from densities in high dimensions is an active research field of Monte Carlo methods in general. Assuming both high dimensionality and computational expensiveness of the target density incurs two nested challenges in the problem setup. We aim to solve one problem at a time, focusing on the case where the target density is computationally expensive but in low dimensions. Still, this case has numerous important applications. For example, the Lorenz weather forecast model depends on a 40-dimensional differential equation in the data domain, while the parameter space is two-dimensional (Wilks, 2005). Another example is a hierarchical model for very large satellite spatial data (Lyne et al., 2015), where the majority of the parameters can be analytically marginalised out, yet a few remaining parameters require sampling.

4 Convergence Analysis

This section establishes the weak convergence of the weighted samples $\{\theta_n^*, w_n^*\}_{n=1}^N$ obtained by Algorithm 1. Firstly, Section 4.1 introduces the definition of maximum mean discrepancy (MMD; Smola et al., 2007; Gretton et al., 2012), which we use as a metric to measure the approximation error between the weighted samples and the target density. Section 4.2 then derives the convergence rate of Algorithm 1 in our default setting where the proposal density is uniform. Section 4.3 provides the convergence rate of Algorithm 1 in a general setting where the proposal density is arbitrary.

4.1 Metric of Convergence

Consider a metric in the space of probability distributions on Θ , which metrises the weak convergence of probability distributions. That is, a probability distribution weakly converges to another if and only if the metric between them converges to zero. A convenient approach to proving the convergence between the BIS samples and the target density p is to show the decay of the metric between them. In this regard, MMD is a computationally and theoretically appealing choice of metric.

MMD is a metric determined by a kernel function $\kappa : \Theta \times \Theta \rightarrow \mathbb{R}$. Recall that, for every kernel, there exists a uniquely associated Hilbert space of functions on Θ , called reproducing kernel Hilbert space (RKHS). See e.g. Paulsen and Raghupathi (2016) for introduction to RKHS. Denote by \mathcal{H}_κ the RKHS of the kernel κ , with the norm denoted $\|\cdot\|_{\mathcal{H}_\kappa}$. MMD is then defined as the worst-case error between two expectations with respect to p and q :

$$d(p, q) := \sup_{\|f\|_{\mathcal{H}_\kappa} \leq 1} \left| \mathbb{E}_{\theta \sim p}[f(\theta)] - \mathbb{E}_{\theta \sim q}[f(\theta)] \right|. \quad (1)$$

MMD satisfies all the axioms of a metric and metrises the weak convergence of probability distributions under mild regularity of the kernel (Simon-Gabriel et al., 2023). For our theoretical analysis, the choice of kernel κ is not particularly crucial. Our convergence bounds do not depend on the

choice of kernel κ up to a condition posited below. If there exists any kernel that satisfies the condition, it suffices for our analysis on the weak convergence of the BIS samples.

A kernel κ is said to be integrally strictly positive definite if $\int_{\Theta \times \Theta} \kappa(\theta, \theta') d\mu(\theta) d\mu(\theta') > 0$ for all finite non-zero signed Borel measures μ on Θ . This is analogue to strictly positive definiteness of kernels. For example, Gaussian kernels satisfy this property (Sriperumbudur et al., 2010). For convenience in our analysis, we posit the following condition on the kernel κ used for MMD. In the condition, all the bounds of the kernel are set to 1 with no loss of generality. This is because, if the bounds of the kernel exceeds 1, we can multiply the kernel by some constant and define a new kernel whose bounds are below 1. Gaussian kernels are a trivial example that meets the condition.

Kernel Condition: The kernel $\kappa : \Theta \times \Theta \rightarrow \mathbb{R}$ is integrally strictly positive definite. The kernel κ admits a factorisation $\kappa(\theta, \theta') = \prod_{i=1}^d \kappa_i(\theta_{(i)}, \theta'_{(i)})$ for some kernels $\kappa_1, \dots, \kappa_d$, where $\theta_{(i)}$ and $\theta'_{(i)}$ denote the i -th coordinate of θ and θ' . For each $i = 1, \dots, d$, the kernel κ_i is uniformly bounded by 1 and admits the derivative $(\partial/\partial\theta_{(i)})(\partial/\partial\theta'_{(i)})\kappa(\theta_{(i)}, \theta'_{(i)})$ uniformly bounded by 1.

4.2 Deterministic Rate in Uniform Case

Our first analysis focuses on the case where the proposal density u is uniform, as discussed in Section 3.2. Strikingly, the uniformity of u results in a deterministic convergence rate, regardless of whether the proposal sequence is random or deterministic. A key quantity in this analysis is the *star discrepancy* D^* of given K points $\{\theta_n\}_{n=1}^K$ in Θ , which we define by

$$D^*(\{\theta_n\}_{n=1}^K) := \sup_{B \in \mathcal{B}} \left| \frac{\#\{\theta_n \in B\}}{K} - \frac{\text{Vol}(B)}{\text{Vol}(\Theta)} \right|$$

where \mathcal{B} is a set of all subboxes in Θ s.t. the left-boundary at every i -th coordinate is equal to that of Θ , $\#\{\theta_n \in B\}$ denotes the number of the points contained in the box B , and $\text{Vol}(\cdot)$ denotes the volume of a given region. Although the star discrepancy is typically defined for points in the unit cube, we use the above definition generalised to the domain Θ .

Denote by $\partial_i f(\theta)$ the partial derivative of a function $f(\theta)$ with respect to the i -th coordinate of the argument θ . Denote by $\partial_{1:d} f(\theta)$ the first mixed partial derivative of a function $f(\theta)$, that is, $\partial_{1:d} f(\theta) = \partial_1 \cdots \partial_d f(\theta)$. In what follows, denote by δ_N the empirical distribution of the N weighted samples $\{\theta_n^*, w_n^*\}_{n=1}^N$ of BIS. We arrive at the main result.

Theorem 1. *Suppose that the target density p admits the first mixed partial derivative $\partial_{1:d} p(\theta)$ that is uniformly continuous. Suppose that the proposal density u is uniform. Given any proposal sequence $\{\theta_n\}_{n=1}^{M+N}$ and criterion U_n , the weighted samples $\{\theta_n^*, w_n^*\}_{n=1}^N$ of Algorithm 1 achieve*

$$d(p, \delta_N) \leq C_1 D^*(\{\theta_n\}_{n=1}^{N+M}) + C_2 \frac{M}{N+M}$$

where C_1 and C_2 are constants dependent only on p and u .

Proof. The proof is provided in Appendix B.2. □

Theorem 1 provides an immediate corollary on an explicit convergence rate of BIS. It suffices to know a choice of the proposal sequence $\{\theta_n\}_{n=1}^{M+N}$ that gives an upper bound of the star discrepancy. The Halton sequence leads to a well-known bound of the star discrepancy (see e.g. Niederreiter, 1992). We obtain the following rate under our default setting in Section 3.2.

Corollary 1. *In the setting of Theorem 1, suppose that the proposal sequence $\{\theta_n\}_{n=1}^{M+N}$ is the scaled Halton sequence in Definition 1. The weighted samples $\{\theta_n^*, w_n^*\}_{n=1}^N$ of Algorithm 1 achieve*

$$d(p, \delta_N) \leq C_1 \frac{\log(N+M)^d}{N+M} + C_2 \frac{M}{N+M}$$

where C_1 and C_2 are constants dependent only on p and u .

Proof. The proof is provided in Appendix B.3. \square

This rate is deterministic and faster than the concentration rate of standard Monte Carlo integration $\mathcal{O}(N^{-1/2})$. Interestingly, even i.i.d random samples from the uniform density u lead to another bound of the star discrepancy, which holds almost surely (Morokoff and Caflisch, 1994). We do not consider this case, as the convergence rate in this case is slower. Still, it is worth noting that the i.i.d random proposal sequence can result in the almost sure convergence of the MMD. Finally, the above convergence rate implies the weak convergence of the weighted samples.

Corollary 2. *Suppose the same setting as Corollary 1. The empirical distribution δ_N of the weighted samples $\{\theta_n^*, w_n^*\}_{n=1}^N$ weakly converges to the target density p as $N \rightarrow \infty$.*

Proof. The proof is provided in Appendix B.6. \square

Notably, the convergence rate is independent of a choice of the criterion U_n . It guarantees that BIS will not worsen the convergence rate of importance sampling. Therefore, a reasonably designed point-selection step in BIS will only accelerate the convergence.

4.3 Concentration Rate in General Case

Our next analysis considers a general setting, where the proposal density u is arbitrary and the proposal sequence $\{\theta_i\}_{i=1}^\infty$ is a sequence of i.i.d. random samples from u . Since the proposal sequence $\{\theta_i\}_{i=1}^\infty$ is stochastic, we derive a concentration rate of the MMD between the weighted samples and the target density.

Theorem 2. *Suppose that the proposal density u is a density uniformly bounded on Θ . Given i.i.d. random samples from u as a proposal sequence $\{\theta_n\}_{n=1}^{M+N}$ and a criterion U_n , the weighted samples $\{\theta_n^*, w_n^*\}_{n=1}^N$ of Algorithm 1 achieve that, for all $0 < \epsilon < 1$,*

$$\mathbb{P} \left(d(p, \delta_N) \leq \frac{C_1 + C_2 \sqrt{\log(2/\epsilon)}}{\sqrt{N+M}} + C_3 \frac{M}{N+M} \right) \geq 1 - \epsilon$$

where \mathbb{P} is a probability taken with respect to the random samples $\theta_1, \dots, \theta_{M+N} \stackrel{i.i.d.}{\sim} u$, and C_1 , C_2 , and C_3 are constants dependent only on p and u .

Proof. The proof is provided in Appendix B.5. \square

We have an immediate corollary on the almost-sure weak convergence of the weighted samples.

Corollary 3. *Suppose the same setting as Theorem 2. The empirical distribution δ_N of the weighted samples $\{\theta_n^*, w_n^*\}_{n=1}^N$ weakly converges to the target density p a.s. as $N \rightarrow \infty$.*

Proof. The proof is provided in Appendix B.6. \square

While this setting allows for any proposal density u , the resulting convergence rate is stochastic and slower than the rate established in Section 4.2. This result also motivates our default setting of the proposal density and the proposal sequence discussed in Section 3.2. This completes the convergence analysis of BIS. Next we provide empirical assessment of the performance of BIS.

5 Empirical Assessment

This section examines the empirical performance of BIS in three distinct experiments. The first experiment concerns three benchmark densities in two dimensions, where we illustrate the samples obtained by BIS, together with the convergence rate. The second experiment considers a weather forecast model from Lorenz (1995), for which Bayesian inference is performed using a synthetic likelihood based on simulations (Hakkarainen et al., 2012). The third experiment focuses on exact Bayesian inference of the g-and-k models (Prangle, 2020), whose density requires a numerical optimisation to be evaluated at each data point. The source codes of the experiments are available in <https://github.com/takuomatsubara/Bandit-Importance-Sampling>.

5.1 Benchmark Densities

We consider three benchmark densities. The first density is a simple unimodal Gaussian density. The second density is a bimodal exponential-family density illustrating a challenging scenario that involves multiple modes and benefits from efficient exploration of the domain. The last density is a banana-shaped density illustrating another challenging scenario that involves a complex tail probability. All the densities are defined in the following form proposed in Järvenpää et al. (2021):

$$p(\theta) \propto \exp \left(-\frac{1}{2} \begin{bmatrix} T_1(\theta) \\ T_2(\theta) \end{bmatrix}^T \begin{bmatrix} 1 & \rho \\ \rho & 1 \end{bmatrix} \begin{bmatrix} T_1(\theta) \\ T_2(\theta) \end{bmatrix} \right),$$

where Appendix D.1 contains the definition of T_1 , T_2 , and ρ for each density. The domain Θ of each density is, respectively, $\Theta = [-16, 16]^2$, $\Theta = [-6, 6]^2$, and $\Theta = [-6, 6] \times [-20, 2]$. The aim of this experiment is to demonstrate the performance of BIS under each benchmark scenario.

By BIS, we obtained 100 weighted samples that approximate each target density. Following Järvenpää et al. (2021), the first 10 points were randomly selected from the Halton sequence, in order to increase stability of the GP surrogate model. The mean and covariance function of the GP prior in GP-UJB were set to, respectively, zero and the Gaussian kernel with its length-scale and variance constants as hyperparameters to tune. The size of the candidate pool M in BIS was fixed to $M = 2048$ for all the densities. See Appendix C.3 for simulation studies on sensitivity of BIS to the size of the candidate pool M . Figure 2 compares each target density and the obtained samples, demonstrating that BIS captures the high probability region of each density. In particular, BIS efficiently tracked down the complex geometry of the bimodal and banana-shaped densities.

We measured the approximation error of the obtained samples by MMD. For computation of the MMD, we approximated each ground-truth target density by standard importance sampling based on 100,000 points from the scaled Halton sequence. We used the 100,000 weighted samples as a sufficiently accurate representation of each target density. Figure 3 shows the MMD between the target density and the BIS samples. For reference, BIS was compared with standard importance

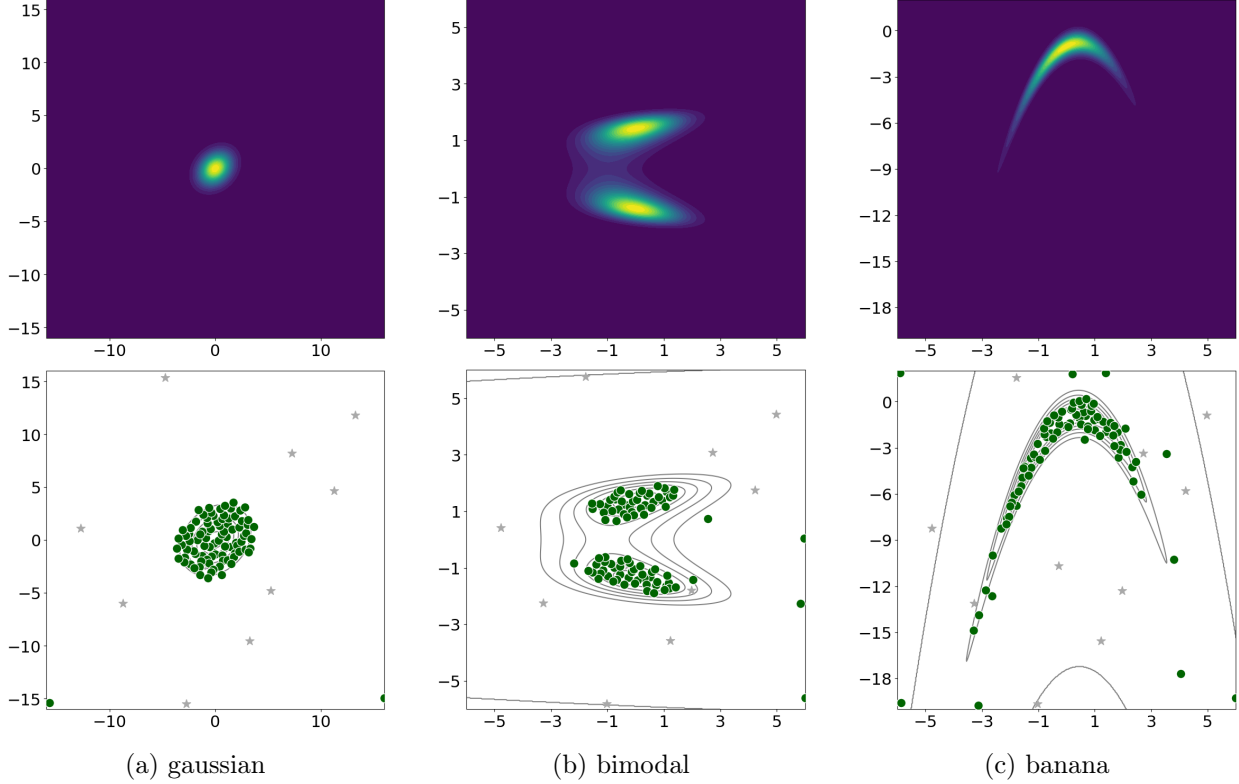


Figure 2: Visualisation of 100 BIS samples obtained for each benchmark density. The top panels show the contour colourmap of each density. The bottom panels show the initial 10 random points (star) and the following 90 points selected by BIS (circle). In the bottom panels, we added the contour plot of each density (solid line), where the contour values of each density were powered to $1/3$ for better visualisation of the curvature of the tail geometry.

sampling, where we obtained samples from the scaled Halton sequence and assigned self-normalised weights to them. Appendix D.1 further shows the number of samples required for standard importance sampling to surpass the approximation error of 100 BIS samples. BIS reduced the number of samples required to achieve the approximation error by nearly 95% on average.

BIS does *not* require the GP surrogate model to converge exactly to the target density, where a reasonable approximation of the target density suffices for guiding sample selection. That said, it may still be instructive to measure the approximation error between the target density and the GP surrogate model used in BIS. We computed the total variation distance (TVD) between the target density and the plug-in density estimator based on the GP mean m_n . Figure 4 demonstrates the decay of the approximation error. The plug-in density estimator of BIS was compared with three other approaches of GP-based density estimators. The first approach is a naive plug-in density estimator based on the GP mean trained on QMC samples. The second approach is a modification of Sinsbeck and Nowak (2017) derived in Järvenpää et al. (2021), called the expected integrated variance (EIV) design. The EIV design is numerically more stable than the original proposal in Sinsbeck and Nowak (2017) since it needs no simulation from the GP posterior. The last approach is the randomised BO of Kim and Sanz-Alonso (2024). Note that the mean and covariance function

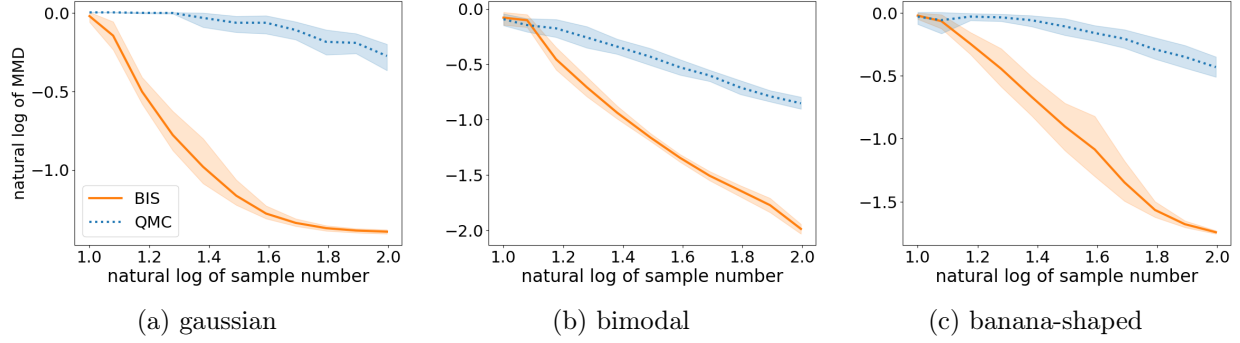


Figure 3: The approximation error of BIS weighted samples (solid line) and importance sampling based on the QMC sequence (dotted line). The experiment was repeated 10 times, where the bold line represents the averaged error and the band represents the 95% confidence interval.

of the GP surrogate model, including the hyperparameter, is the same in each method, where the only difference is in the input points on which the GP is trained. The GP surrogate model trained on the weighted samples of BIS achieves the least error in all the cases.

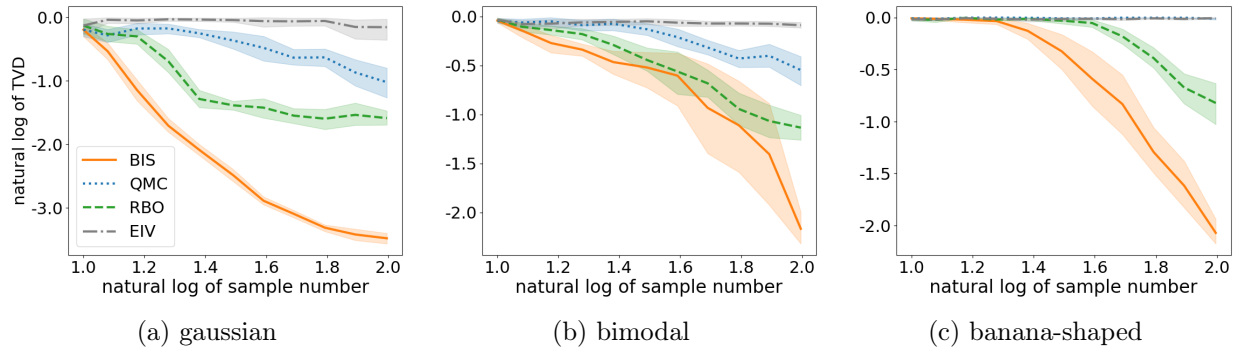


Figure 4: The approximation error of the GP-based density estimator trained on BIS samples (solid line), the QMC sequence (dotted line), points by the randomised BO (dashed line), and points by the EIV design (dash-dotted line). The experiment was repeated 10 times, where the bold line represents the averaged error and the band represents the 95% confidence interval.

5.2 Lorenz Weather Model

Wilks (2005) proposed a modification of the celebrated Lorenz dynamical system for weather forecast (Lorenz, 1995). They assumed that the weather dynamical system has ‘slow’ and ‘fast’ variables, where the former is observable at weather stations and the latter is unobservable. The modified Lorenz model includes a stochastic noise that represents the influence of the unobservable variables. It consists of 40 observable variables $(x_1(t), \dots, x_{40}(t)) \in \mathbb{R}^{40}$ dependent on time t , whose dynamics is described by the following differential equation

$$\frac{d}{dt}x_k(t) = -x_{k-1}(t)(x_{k-2}(t) - x_{k+1}(t)) - x_k(t) + 10 - \theta_1 - \theta_2 x_k(t) + \eta_k(t) \quad (2)$$

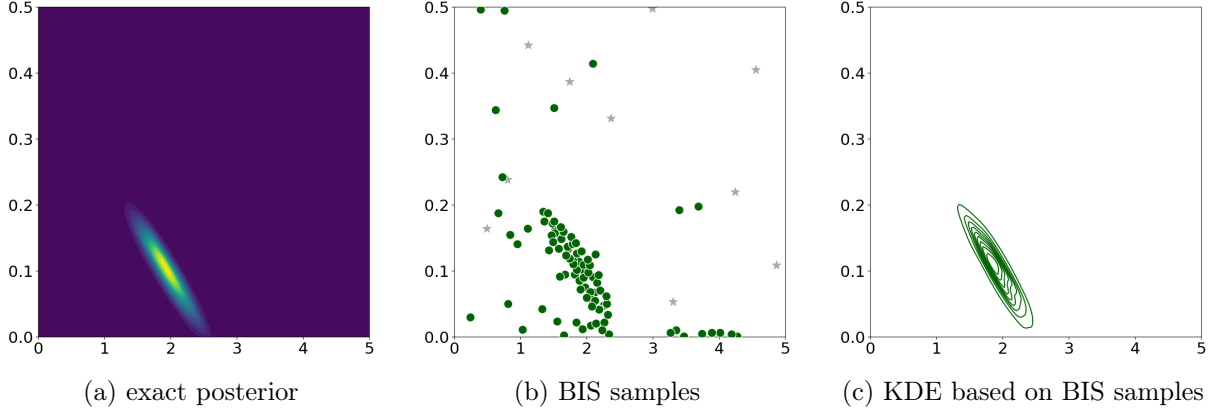


Figure 5: Visualisation of 100 BIS samples for the Lorentz weather model. The left panel is the contour colourmap of the target posterior. The middle panel shows the locations of the initial 10 random points (star) and the following 90 points selected by BIS (circle). The right panel shows the contour colourmap of the KDE of the 100 weighted samples.

where $\theta := (\theta_1, \theta_2) \in \mathbb{R}^2$ is the parameter that determines the system, and $\eta_k(t)$ is the stochastic noise that shall be defined below. Here, the index k of each variable is an integer modulo 40, meaning that $k - 1 = 40$ and $k - 2 = 39$ when $k = 1$, and that $k + 1 = 1$ when $k = 40$. We suppose that the model is defined over the time interval $[0, 4]$.

We consider a setting where the initial state of the 40 variables at time $t = 0$ is known and the subsequent state of the 40 variables is observed for 20 days on a daily basis. One day corresponds to the time duration 0.2 in this model. Hence, we observe a sample path of the 40 variables at 20 time indices equispaced in the interval $[0, 4]$, starting from the known initial state at $t = 0$. To simulate sample paths of the model, we solve the differential equation (2) by the 4th-order Runge-Kutta method with a small time step $\delta t = 0.025$, as in Thomas et al. (2022). Wilks (2005) assumed that the stochastic noise, for each k , has the following first-order autoregressive structure

$$\eta_k(t + \delta t) = \phi \eta_k(t) + \sqrt{1 - \phi^2} \epsilon_k(t)$$

where $\phi \in [0, 1]$ is set to 0.4 throughout, and $\epsilon_k(t)$ is a standard normal noise drawn independently at each time t . The initial value of the noise $\eta_k(0)$ is given by $\sqrt{1 - \phi^2} \epsilon_k(0)$. For our experiment, we sampled the initial state of the 40 variables from a standard normal distribution. We then simulated the sample path observed at the 20 time indices under the parameter $(\theta_1, \theta_2) = (2.0, 0.1)$.

Hakkarainen et al. (2012) suggested to use a synthetic likelihood to perform Bayesian inference of the Lorentz weather model; see e.g. Frazier et al. (2023) for introduction of synthetic likelihoods. Appendix D.2 details the summary statistics used for the synthetic likelihood in this experiment. Our aim is to sample from the posterior defined by the synthetic likelihood and a prior. We specified a uniform prior on the parameter domain $\Theta = [0.0, 5.0] \times [0.0, 0.5]$, following Järvenpää et al. (2021). At each θ , the synthetic likelihood is computed using 10,000 sample paths that are sufficiently many so that the estimation error of the synthetic likelihood is negligible. For BIS, we used the same setting in Section 5.1. Figure 5 shows 100 samples obtained by BIS, together with a kernel density estimator (KDE) based on the weighted samples. For comparison, we applied standard importance sampling to the target posterior, where we used the 10,000 scaled Halton sequence as samples and assigned self-normalised importance weights to them. Figure 5 visualises the target posterior, using

the KDE based on that 10,000 weighted samples as a sufficiently accurate representation of the target density. Figure 5 illustrates that the weighted samples of BIS, visualised by the KDE, recover the target posterior well. To verify that, we evaluated the MMD between the target posterior and the 100 weighted samples of BIS, where the reported value of the MMD was 0.008.

5.3 G-and-K Model

The g-and-k model is an expressive parametric family that can model the location, scale, shape, and skewness of data. Notable applications of the g-and-k model include modelling of foreign exchange return data that can exhibit heavy-tail and skewed behaviours (Prangle, 2020). The g-and-k model on \mathbb{R} is parametrised by a four-dimensional parameter $\theta = (\theta_1, \theta_2, \theta_3, \theta_4) \in \mathbb{R}^4$. Only a quantile function $Q(u | \theta)$ of the model is analytical, where

$$Q(u | \theta) = \theta_1 + \theta_2 z(u) (1 + c \tanh(0.5 \theta_3 z(u))) (1 + z(u)^2)^{\theta_4}$$

for $u \in (0, 1)$. Here c is a hyperparameter that we set to 0.8.

Denote by $Q'(u | \theta)$ the derivative of the quantile function with respect to u . Denote by $Q(x | \theta)^{-1}$ the inverse of the quantile function $x = Q(u | \theta)$, that is, $u = Q(x | \theta)^{-1}$. Rayner and MacGillivray (2002) showed that the density of the g-and-k model is equal to

$$p(x | \theta) = \frac{1}{Q'(Q(x | \theta)^{-1} | \theta)}.$$

However, this density is not available in closed form because the inverse $Q(x | \theta)^{-1}$ can be only numerically available. This makes the evaluation of the log-likelihood computationally expensive, as it requires numerical optimisation to compute the inverse $Q(x | \theta)^{-1}$ at each x and θ . ABC is arguably the most common approach to approximate Bayesian inference of the g-and-k model. Samples drawn by ABC follow an approximation of the exact posterior, involving a drawback to overestimate the variance of the posterior. In contrast, BIS performs exact Bayesian inference, targeting the exact posterior.

We simulated 1000 data points $\{x_i\}_{i=1}^{1000}$ from the g-and-k model $p(x | \theta_0)$ under the parameter $\theta_0 = (3, 1, 2, 0.5)$. The domain Θ is the hyperrectangle $[0, 10]^4$ and a uniform prior on Θ is used to define the posterior. By BIS, we obtained 400 weighted samples of the posterior, where the first 40 points were randomly selected from the Halton sequence to increase stability of the GP surrogate model. In high dimensions, modes of probability measures with no sufficient tail decay can concentrate around the boundary of the domain, as known in the concentration on the sphere phenomenon. In this experiment, the mean function of the GP prior in GP-UJB was set to a quadratic polynomial whose coefficients are the hyperparameter, so that a sufficient tail decay is encoded in the surrogate density. The covariance kernel was set to the Gaussian kernel with length-scale 1 and variance 20, where the large variance assists in driving exploration of GP-UJB and avoiding overfitting of the surrogate density. The size of the candidate pool M was fixed to $M = 320,000$. Figure 6 shows a histogram of the 400 samples of BIS in each coordinate of the parameter. Figure 6 further shows a KDE constructed from the 400 weighted samples of BIS. BIS was compared with the KDE constructed from the 320,000 scaled Halton sequence with self-normalised importance weights assigned. It demonstrates that the weighted samples of BIS recovers the target posterior, placing a probability mass correctly around the true parameter θ_0 .

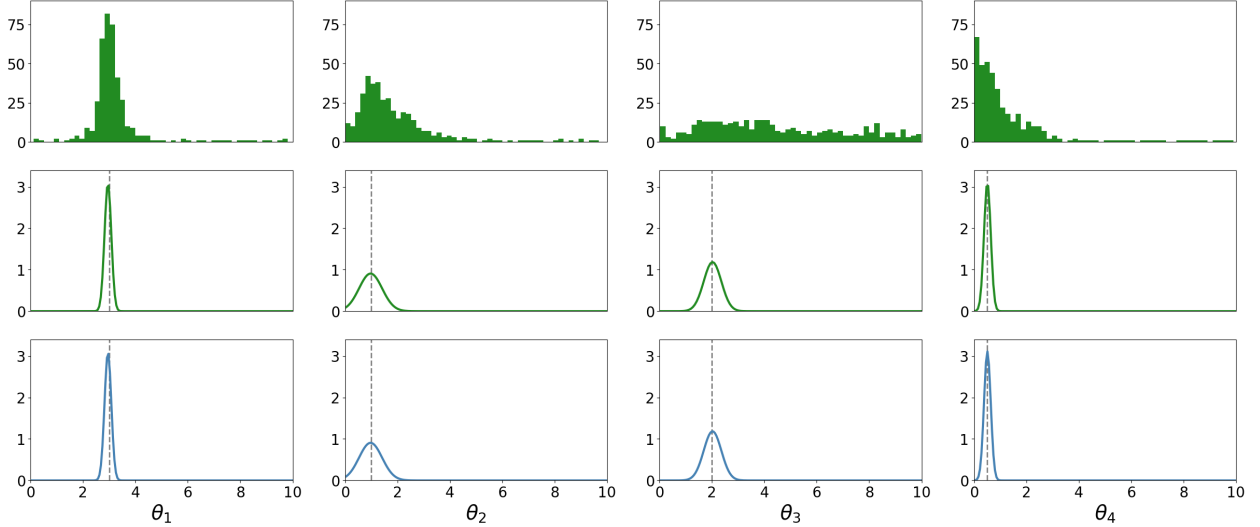


Figure 6: Visualisation of 400 weighted samples of BIS for the g-and-k model. The top panels are the histograms of the samples of BIS in each coordinate of the parameter $\theta = (\theta_1, \theta_2, \theta_3, \theta_4)$. The middle panels show the KDEs based on the weighted samples of BIS in each coordinate. The bottom panels show the marginal posteriors in each coordinate estimated by the KDEs based on the 320,000 weighted samples. The dotted line indicates the location of the correct parameter.

6 Related Work

To the best of the authors’ knowledge, BIS is the first method to frame the design of samples in sampling as a bandit problem. This work leveraged GP surrogate modelling of the target density to guide the design of samples adaptively. BIS allows for the convergence of the designed samples. This is in contrast to most existing works on experimental designs for GPs, in which the designed points are used only as training inputs of GP surrogate models.

Sinsbeck and Nowak (2017) proposed a GP surrogate model of the likelihood for efficient approximation of the posterior. They developed a sequential experimental design of points, at which the likelihood is evaluated for training of the GP surrogate model. Their approach is to find an estimator of the log-likelihood that minimises a Bayes risk associated with the GP surrogate model at each iteration. They then select a point that maximises the Bayes estimator of the likelihood. Once the specified number of points has been obtained, the posterior is approximated by a so-called “plug-in” posterior, in which the log-likelihood is replaced by the GP posterior mean. Järvenpää et al. (2021) extended the approach of Sinsbeck and Nowak (2017), considering a GP surrogate model of the posterior directly. They proposed a batched sequential design that selects a few points simultaneously at each iteration. However, their approaches draw on several heuristics and do not guarantee convergence of the GP surrogate model theoretically.

Recently, Kim and Sanz-Alonso (2024) proposed a simple modification of BO. Their approach is to include an extra random point in the training dataset of GP at each iteration. They applied the modified BO for maximum-a-posteriori estimation of the posterior, setting the objective function to the logarithm of the posterior. They showed that the mean function of the GP posterior used in the modified BO converges to the target posterior if the GP prior is well specified. That result is natural because adding random samples to the training dataset ensures that the target posterior is eventually

evaluated everywhere in the domain. Nonetheless, the result offers an inspiring implication that imposing a certain restriction, by which points acquired by BO eventually fill the domain of interest, is sufficient to guarantee convergence of the GP surrogate model to the posterior.

Applications of GP surrogate modelling in Bayesian computation are not limited to approximation of the posterior density. Osborne et al. (2012) and Gunter et al. (2014) proposed a GP-based active learning framework to compute the model evidence. Meeds and Welling (2014) accelerated approximation Bayesian computation (ABC) with GP modelling of summary statistics. Gutmann and Corander (2016) developed an experimental design for GP modelling of discrepancy measures in ABC. Nemeth and Sherlock (2018) leveraged GP modelling to merge multiple posteriors conditional on different subsets of data. Bai et al. (2024) proposed a physics-informed GP surrogate model of forward simulators in Bayesian inverse problems.

7 Conclusion

Sampling from black-box densities has increasingly been a common task, for example, in Bayesian inference of complex models. However, there has been little existing literature on particle-based sampling methods tailored for black-box densities. This paper introduced BIS, the first importance sampling approach to black-box densities, which frames the design of samples as a bandit problem.

BIS is a simple and powerful sampling framework built on a choice of the proposal sequence and the point-selection criterion. This paper introduced our default point-selection criterion, GP-UJB, based on GP surrogate models of target densities. GP-UJB admits a decomposition into two terms that drive exploration of new points and exploitation of past information. On a theoretical level, we established the weak convergence of the weighted samples obtained by BIS. The empirical performance of BIS was demonstrated using benchmark densities and real-world models.

In the general framework of BIS, a choice of the point-selection criterion is flexible, whereas we focused on GP-UJB in this paper. As mentioned in Section 3, difficulty in applying GPs in high dimensions is a well-known open challenge. GP-UJB inherits the same challenge for BIS. Designing point-selection criteria suitable for high-dimensional densities requires further substantial studies. Promising directions of future research include such new designs of point-selection criteria beyond the scope of GP surrogate modelling.

References

- T. Bai, A. L. Teckentrup, and K. C. Zygalakis. Gaussian processes for Bayesian inverse problems associated with linear partial differential equations. *Statistics and Computing*, 34(4):139, 2024.
- M. A. Beaumont, W. Zhang, and D. J. Balding. Approximate Bayesian computation in population genetics. *Genetics*, 162(4):2025–2035, 2002.
- J. Besag. On the statistical analysis of dirty pictures. *Journal of the Royal Statistical Society. Series B (Methodological)*, 48(3):259–302, 1986.
- S. Brooks, A. Gelman, G. Jones, and X. Meng. *Handbook of Markov Chain Monte Carlo*. Chapman and Hall/CRC, 1st edition edition, 2011.

- M. F. Bugallo, V. Elvira, L. Martino, D. Luengo, J. Miguez, and P. M. Djuric. Adaptive importance sampling: the past, the present, and the future. *IEEE Signal Processing Magazine*, 34(4):60–79, 2017.
- A. D. Bull. Convergence rates of efficient global optimization algorithms. *Journal of Machine Learning Research*, 12(88):2879–2904, 2011.
- M.-H. Chen, P. Müller, D. Sun, K. Ye, and D. K. Dey. *Frontiers of Statistical Decision Making and Bayesian Analysis*. Springer, 2010.
- C. Cotter, S. Cotter, and P. Russell. Ensemble transport adaptive importance sampling. *SIAM/ASA Journal on Uncertainty Quantification*, 7(2):444–471, 2019.
- S. L. Cotter, I. G. Kevrekidis, and P. T. Russell. Transport map accelerated adaptive importance sampling, and application to inverse problems arising from multiscale stochastic reaction networks. *SIAM/ASA Journal on Uncertainty Quantification*, 8(4):1383–1413, 2020.
- J. Dick and F. Pillichshammer. *Digital Nets and Sequences: Discrepancy Theory and Quasi-Monte Carlo Integration*. Cambridge University Press, 2010.
- P. J. Diggle. A point process modelling approach to raised incidence of a rare phenomenon in the vicinity of a prespecified point. *Journal of the Royal Statistical Society. Series A (Statistics in Society)*, 153(3):349–362, 1990.
- D. T. Frazier, D. J. Nott, C. Drovandi, and R. Kohn. Bayesian inference using synthetic likelihood: asymptotics and adjustments. *Journal of the American Statistical Association*, 118(544):2821–2832, 2023.
- M. Girolami. Bayesian inference for differential equations. *Theoretical Computer Science*, 408(1):4–16, 2008.
- S. M. Goodreau, J. A. Kitts, and M. Morris. Birds of a feather, or friend of a friend? using exponential random graph models to investigate adolescent social networks. *Demography*, 46(1):103–125, 2009.
- R. B. Gramacy. *Surrogates*. Chapman and Hall/CRC, 1st edition edition, 2020.
- A. Gretton, K. M. Borgwardt, M. J. Rasch, B. Schölkopf, and A. Smola. A kernel two-sample test. *Journal of Machine Learning Research*, 13(25):723–773, 2012.
- T. Gunter, M. A. Osborne, R. Garnett, P. Hennig, and S. J. Roberts. Sampling for inference in probabilistic models with fast Bayesian quadrature. In *Proceedings of the 28th International Conference on Neural Information Processing Systems*, volume 2, page 2789–2797, 2014.
- M. U. Gutmann and J. Corander. Bayesian optimization for likelihood-free inference of simulator-based statistical models. *Journal of Machine Learning Research*, 17(125):1–47, 2016.
- J. Hakkarainen, A. Ilin, A. Solonen, M. Laine, H. Haario, J. Tamminen, E. Oja, and H. Järvinen. On closure parameter estimation in chaotic systems. *Nonlinear Processes in Geophysics*, 19(1):127–143, 2012.

- J. Halton. Algorithm 247: radical-inverse quasi-random point sequence. *Communications of the ACM*, 7(12):701–702, 1964.
- J. M. Hammersley and K. W. Morton. Poor man’s monte carlo. *Journal of the Royal Statistical Society. Series B (Methodological)*, 16(1):23–38, 1954.
- M. Järvenpää, M. U. Gutmann, A. Vehtari, and P. Marttinen. Parallel Gaussian process surrogate Bayesian inference with noisy likelihood evaluations. *Bayesian Analysis*, 16(1):147–178, 2021.
- M. Kanagawa, P. Hennig, D. Sejdinovic, and B. K. Sriperumbudur. Gaussian processes and kernel methods: a review on connections and equivalences. *arXiv: 1807.02582*, 2018.
- H. Kim and D. Sanz-Alonso. Enhancing Gaussian process surrogates for optimization and posterior approximation via random exploration. *arXiv: 2401.17037*, 2024.
- E. N. Lorenz. Predictability: a problem partly solved. *Seminar on Predictability*, 1:1–18, 1995.
- A.-M. Lyne, M. Girolami, Y. Atchadé, H. Strathmann, and D. Simpson. On Russian roulette estimates for Bayesian inference with doubly-intractable likelihoods. *Statistical Science*, 30(4): 443–467, 2015.
- J.-M. Marin, P. Pudlo, C. P. Robert, and R. J. Ryder. Approximate Bayesian computational methods. *Statistics and Computing*, 22(6):1167–1180, 2012.
- E. Meeds and M. Welling. GPS-ABC: Gaussian process surrogate approximate Bayesian computation. In *Proceedings of the Thirtieth Conference on Uncertainty in Artificial Intelligence*, page 593–602, 2014.
- J. Mockus. *Bayesian Approach to Global Optimization: Theory and Applications*. Springer, 1989.
- W. J. Morokoff and R. E. Caflisch. Quasi-random sequences and their discrepancies. *SIAM Journal on Scientific Computing*, 15(6):1251–1279, 1994.
- C. Nemeth and C. Sherlock. Merging MCMC subposteriors through Gaussian-process approximations. *Bayesian Analysis*, 13(2):507–530, 2018.
- H. Niederreiter. *Random Number Generation and Quasi-Monte Carlo Methods*. Society for Industrial and Applied Mathematics, 1992.
- M. Osborne, R. Garnett, Z. Ghahramani, D. K. Duvenaud, S. J. Roberts, and C. Rasmussen. Active learning of model evidence using Bayesian quadrature. In *Advances in Neural Information Processing Systems*, volume 25, 2012.
- V. I. Paulsen and M. Raghupathi. *An Introduction to the Theory of Reproducing Kernel Hilbert Spaces*. Cambridge University Press, 2016.
- D. Prangle. Gk: an r package for the g-and-k and generalised g-and-h distributions. *The R Journal*, 12(1):7–20, 2020.
- C. E. Rasmussen and C. K. I. Williams. *Gaussian Processes for Machine Learning*. The MIT Press, 2005.

- G. D. Rayner and H. L. MacGillivray. Numerical maximum likelihood estimation for the g-and-k and generalized g-and-h distributions. *Statistics and Computing*, 12(1):57–75, 2002.
- H. Rue and L. Held. *Gaussian Markov Random Fields: Theory and Applications*. Chapman and Hall/CRC, 1st edition edition, 2005.
- B. Shahriari, K. Swersky, Z. Wang, R. P. Adams, and N. de Freitas. Taking the human out of the loop: a review of Bayesian optimization. *Proceedings of the IEEE*, 104(1):148–175, 2016.
- C.-J. Simon-Gabriel, A. Barp, B. Schölkopf, and L. Mackey. Metrizing weak convergence with maximum mean discrepancies. *Journal of Machine Learning Research*, 24(184):1–20, 2023.
- M. Sinsbeck and W. Nowak. Sequential design of computer experiments for the solution of Bayesian inverse problems. *SIAM/ASA Journal on Uncertainty Quantification*, 5(1):640–664, 2017.
- A. Smola, A. Gretton, L. Song, and B. Schölkopf. A Hilbert space embedding for distributions. In *Algorithmic Learning Theory*, pages 13–31, 2007.
- N. Srinivas, A. Krause, S. Kakade, and M. Seeger. Gaussian process optimization in the bandit setting: no regret and experimental design. In *Proceedings of the 27th International Conference on International Conference on Machine Learning*, page 1015–1022, 2010.
- B. K. Sriperumbudur, A. Gretton, K. Fukumizu, B. Schölkopf, and G. R. Lanckriet. Hilbert space embeddings and metrics on probability measures. *Journal of Machine Learning Research*, 11(50):1517–1561, 2010.
- I. Steinwart and A. Christmann. *Support Vector Machines*. Springer, 2008.
- O. Thomas, R. Dutta, J. Corander, S. Kaski, and M. U. Gutmann. Likelihood-free inference by ratio estimation. *Bayesian Analysis*, 17(1):1–31, 2022.
- S. T. Tokdar and R. E. Kass. Importance sampling: a review. *WIREs Computational Statistics*, 2(1):54–60, 2010.
- M. J. Wainwright. *High-Dimensional Statistics: A Non-Asymptotic Viewpoint*. Cambridge University Press, 2019.
- D. J. Warne, R. E. Baker, and M. J. Simpson. A practical guide to pseudo-marginal methods for computational inference in systems biology. *Journal of Theoretical Biology*, 496:110255, 2020.
- D. S. Wilks. Effects of stochastic parametrizations in the Lorenz ’96 system. *Quarterly Journal of the Royal Meteorological Society*, 131(606):389–407, 2005.

Appendix

This appendix contains details of the results presented in the main text. Appendix A presents preliminary lemmas useful for subsequent proofs. Appendix B provides proofs of all the theoretical results presented in the main text. Appendix C delivers simulation studies on the settings of BIS. Appendix D describes additional details of the experiments. It is convenient to introduce the following multi-index notations that will be used throughout.

Notations Let $\alpha = (\alpha_1, \dots, \alpha_d)$ be a d -dimensional vector of binary values, that is, $\alpha \in \{0, 1\}^d$. We call α a binary multi-index. Let $|\alpha|$ be the number of non-zero elements of α . Recall that ∂_i denotes the partial derivative of a function with respect to the i -th coordinate of the argument. Let ∂_i^0 be an identity operator and let ∂_i^1 be the partial derivative ∂_i . Denote by ∂^α the mixed partial derivative $\partial^\alpha = \partial_1^{\alpha_1} \dots \partial_d^{\alpha_d}$. Denote by θ^α a $|\alpha|$ -dimensional vector consisting of all i -th coordinates of θ such that $\alpha_i = 1$. Denote by Θ^α a set of all values of θ^α . Denote by θ_\star^α a d -dimensional vector s.t. the i -th coordinate is equal to that of θ if $\alpha_i = 1$ or fixed to a constant b_i otherwise, where b_i denotes the right boundary of the i -th coordinate of the hyperrectangular domain Θ .

A Preliminary Lemmas

This section contains preliminary lemmas on RKHS and the star discrepancy, which will be useful for the subsequent proofs in Appendix B.

A.1 Preliminary Lemmas on RKHS

Recall that κ is the kernel used for MMD, which meets the kernel condition presented in Section 4. Denote by $\langle \cdot, \cdot \rangle_{\mathcal{H}_\kappa}$ the inner product of the RKHS \mathcal{H}_κ of the kernel κ . Any function f in the RKHS \mathcal{H}_κ satisfies an identity called the *reproducing property* s.t.

$$f(\theta) = \langle f(\cdot), \kappa(\cdot, \theta) \rangle_{\mathcal{H}_\kappa}$$

at each θ pointwise (Steinwart and Christmann, 2008, Section 4.2). The reproducing property also applies to the kernel κ itself, where it holds that $\kappa(\theta, \theta') = \langle \kappa(\cdot, \theta), \kappa(\cdot, \theta') \rangle_{\mathcal{H}_\kappa}$ at each θ, θ' pointwise. We have the following useful lemma on a uniform bound of functions in \mathcal{H}_κ .

Lemma 1. *Any function $f \in \mathcal{H}_\kappa$ s.t. $\|f\|_{\mathcal{H}_\kappa} \leq 1$ satisfies that*

$$\sup_{\theta \in \Theta} |f(\theta)| \leq 1.$$

Proof. By the reproducing property and the Cauchy-Schwartz inequality, we have

$$|f(\theta)| \leq \|f\|_{\mathcal{H}_\kappa} \|\kappa(\cdot, \theta)\|_{\mathcal{H}_\kappa} = \|f\|_{\mathcal{H}_\kappa} \sqrt{\kappa(\theta, \theta)} \leq 1$$

since the kernel κ is bounded by 1 under the kernel condition in Section 4. □

We have another useful lemma on a uniform bound of the mixed partial derivative of functions in \mathcal{H}_κ . Recall that ∂_i denotes the partial derivative with respect to the i -th coordinate of the argument θ , and that ∂^α denotes the mixed partial derivative specified by a given binary multi-index $\alpha \in \{0, 1\}^d$. Denote by $\partial_i \kappa(\theta, \theta')$ and $\partial'_i \kappa(\theta, \theta')$ the partial derivative of $\kappa(\theta, \theta')$ with respect to the i -th coordinate of, respectively, the first argument θ and the second argument θ' .

Lemma 2. *Any function $f \in \mathcal{H}_\kappa$ s.t. $\|f\|_{\mathcal{H}_\kappa} \leq 1$ satisfies that*

$$\sup_{\theta \in \Theta} |\partial^\alpha f(\theta)| \leq 1$$

for all binary multi-index $\alpha \in \{0, 1\}^d$.

Proof. Let I_α be a set of indices i s.t. $\alpha_i = 1$. Similarly, let $I_{\setminus\alpha}$ be a set of indices i s.t. $\alpha_i = 0$. The mixed partial derivative ∂^α can be expressed as $\partial^\alpha = \prod_{i \in I_\alpha} \partial_i$ using the set I_α . Corollary 4.36 of Steinwart and Christmann (2008) implies that

$$|\partial^\alpha f(\theta)| \leq \|f\|_{\mathcal{H}_\kappa} \sqrt{\prod_{i \in I_\alpha} \partial_i \partial'_i \kappa(\theta, \theta)}.$$

It follows from $\|f\|_{\mathcal{H}_\kappa} \leq 1$ and the factorisation $\kappa(\theta, \theta') = \prod_{i=1}^d \kappa_i(\theta_{(i)}, \theta'_{(i)})$ that

$$|\partial^\alpha f(\theta)| \leq \sqrt{\prod_{i \in I_{\setminus\alpha}} \kappa_i(\theta_{(i)}, \theta_{(i)})} \sqrt{\prod_{i \in I_\alpha} \partial_i \partial'_i \kappa_i(\theta_{(i)}, \theta_{(i)})}.$$

Recall the kernel condition that every κ_i is bounded by 1 and admits the derivative $\partial_i \partial'_i \kappa_i(\theta_{(i)}, \theta'_{(i)})$ uniformly bounded by 1. Therefore we have

$$\sup_{\theta \in \Theta} |\partial^\alpha f(\theta)| \leq \sup_{\theta \in \Theta} \sqrt{\prod_{i \in I_{\setminus\alpha}} \kappa_i(\theta_{(i)}, \theta_{(i)})} \sqrt{\prod_{i \in I_\alpha} \partial_i \partial'_i \kappa_i(\theta_{(i)}, \theta_{(i)})} \leq 1.$$

This concludes the proof since the upper bound does not depend on a choice of α . \square

A.2 Preliminary Lemmas on Star Discrepancy

We defined the star discrepancy D^* for points in the domain Θ in the main text. Typically, the star discrepancy is defined for points in the unit cube $[0, 1]^d$. We shall see that the star discrepancy D^* defined for the domain Θ is equivalent to that defined for the unit cube $[0, 1]^d$. To distinguish the two star discrepancies, let D^\dagger be the star discrepancy for the unit cube $[0, 1]^d$. For a given sequence of K points $\{\eta_i\}_{i=1}^K$ in the unit cube $[0, 1]^d$, the latter star discrepancy D^\dagger is defined as follows:

$$D^\dagger(\{\eta_n\}_{n=1}^K) := \sup_{B_0 \in \mathcal{B}_0} \left| \frac{\#\{\eta_n \in B_0\}}{K} - \text{Vol}(B_0) \right| \quad (3)$$

where \mathcal{B}_0 is a set of all subboxes contained in $[0, 1]^d$ s.t. the left-boundary at every i -th coordinate is 0, and $\#\{\eta_n \in B_0\}$ denotes the number of points contained in a box $B_0 \in \mathcal{B}_0$. Notice that the former star discrepancy D^* introduced in the main text is a generalisation of the above definition of the latter D^\dagger , where they coincide with each other when $\Theta = [0, 1]^d$.

Consider a bijective affine map $\tau : [0, 1]^d \rightarrow \Theta$ between the unit cube $[0, 1]^d$ and the domain Θ . Since Θ is hyperrectangular, the bijective affine map τ always exists uniquely. Now we formally state the equivalence of one star discrepancy D^* to the other D^\dagger under the map τ .

Lemma 3. Let $\{\eta_n\}_{n=1}^K$ be the image of a given sequence of points $\{\theta_n\}_{n=1}^K$ in Θ under the map τ^{-1} , that is, each point satisfies $\eta_n = \tau^{-1}(\theta_n)$. It holds for any sequence $\{\theta_n\}_{n=1}^K$ that

$$D^*(\{\theta_n\}_{n=1}^K) = D^\dagger(\{\eta_n\}_{n=1}^K).$$

Proof. Recall that $\#\{\eta_n \in B_0\}$ denotes the number of points contained in a box $B_0 \in \mathcal{B}_0$. The number is invariant to the transform τ , meaning that $\#\{\eta_n \in B_0\} = \#\{\tau(\eta_n) \in \tau(B_0)\}$, where we denote by $\tau(C)$ the image of a subset C of $[0, 1]^d$ under the map τ . Thus, the star discrepancy $D^\dagger(\{\eta_n\}_{n=1}^K)$ on the right-hand side can be expressed as

$$D^\dagger(\{\eta_n\}_{n=1}^K) = \sup_{B_0 \in \mathcal{B}_0} \left| \frac{\#\{\tau(\eta_n) \in \tau(B_0)\}}{K} - \frac{\text{Vol}(B_0)}{\text{Vol}([0, 1]^d)} \right|.$$

The ratio between the volume $\text{Vol}(B_0)$ and $\text{Vol}([0, 1]^d)$ is invariant to the transform τ , meaning that

$$\frac{\text{Vol}(B_0)}{\text{Vol}([0, 1]^d)} = \frac{\text{Vol}(\tau(B_0))}{\text{Vol}(\tau([0, 1]^d))} = \frac{\text{Vol}(\tau(B_0))}{\text{Vol}(\Theta)}$$

Let \mathcal{B} be all subboxes contained in Θ s.t. the left-boundary at every i -th coordinate is equal to that of Θ . Notice that the map τ defines the bijection between the set \mathcal{B}_0 of subboxes in $[0, 1]^d$ and the set \mathcal{B} of subboxes in Θ . This means that we have $\sup_{B_0 \in \mathcal{B}_0} f(\tau(B_0)) = \sup_{B \in \mathcal{B}} f(B)$ for any function f that takes a box in \mathcal{B} as an argument. Therefore, we have

$$D^\dagger(\{\eta_n\}_{n=1}^K) = \sup_{B_0 \in \mathcal{B}_0} \left| \frac{\#\{\tau(\eta_n) \in \tau(B_0)\}}{K} - \frac{\text{Vol}(\tau(B_0))}{\text{Vol}(\Theta)} \right| = \sup_{B \in \mathcal{B}} \left| \frac{\#\{\theta_n \in B\}}{K} - \frac{\text{Vol}(B)}{\text{Vol}(\Theta)} \right|$$

where we used $\theta_n = \tau(\eta_n)$. This concludes the proof. \square

B Proofs

This section contains proofs of all the theoretical results presented in the main text.

B.1 Proof of Proposition 1

Proof. Let $(\star) := \int_{\Theta} |U_n(\theta) - q(\theta)|^2 d\theta$. By the definition of U_n and q , the term (\star) is written as

$$(\star) = \int_{\Theta} \left| \mathbb{E}_{f \sim \mathcal{GP}(m_n, k_n)} [\phi(f(\theta))] - \phi(g(\theta)) \right|^2 d\theta = \int_{\Theta} \left| \mathbb{E}_{f \sim \mathcal{GP}(m_n, k_n)} [\phi(f(\theta)) - \phi(g(\theta))] \right|^2 d\theta.$$

It then follows from the Jensen's inequality that

$$(\star) \leq \int_{\Theta} \left(\underbrace{\mathbb{E}_{f \sim \mathcal{GP}(m_n, k_n)} [|\phi(f(\theta)) - \phi(g(\theta))|]}_{=:(*)} \right)^2 d\theta.$$

We shall upper bound the term $(*)$ at each θ . The derivative ϕ' of ϕ is monotonically non-decreasing because ϕ is a convex function. By the mean value inequality, it holds for all $a, b \in \mathbb{R}$ that

$$|\phi(a) - \phi(b)| \leq \left(\sup_{c \in [a, b]} |\phi'(c)| \right) |b - a| \leq \max(|\phi'(a)|, |\phi'(b)|) |b - a|$$

where the second inequality follows from monotonicity of ϕ' . It thus holds at each θ that

$$\begin{aligned} (*) &\leq \mathbb{E}_{f \sim \mathcal{GP}(m_n, k_n)} \left[\max(|\phi'(f(\theta))|, |\phi'(g(\theta))|) |f(\theta) - g(\theta)| \right] \\ &\leq \mathbb{E}_{f \sim \mathcal{GP}(m_n, k_n)} \left[\underbrace{\max(\exp(f(\theta)), \exp(g(\theta)))}_{=:(**)} |f(\theta) - g(\theta)| \right] \end{aligned}$$

where we used the assumption $|\phi'(\cdot)| \leq \exp(\cdot)$ for the last inequality. It then follows from the Cauchy-Schwartz inequality applied for the expectation that

$$(*) \leq \left(\mathbb{E}_{f \sim \mathcal{GP}(m_n, k_n)} [(**)^2] \mathbb{E}_{f \sim \mathcal{GP}(m_n, k_n)} [|f(\theta) - g(\theta)|^2] \right)^{\frac{1}{2}}. \quad (4)$$

Observe the following trivial inequality

$$(**)^2 = \max(\exp(2f(\theta)), \exp(2g(\theta))) \leq \exp(2f(\theta)) + \exp(2g(\theta)).$$

Notice that, since f is a sample path of the Gaussian process, the point evaluation $f(\theta)$ at each θ follows the Gaussian distribution $\mathcal{N}(m_n(\theta), k_n(\theta, \theta))$. It thus admits the following analytical expectation $\mathbb{E}_{f \sim \mathcal{GP}(m_n, k_n)} [\exp(2f(\theta))] = \exp(2m_n(\theta) + 2k_n(\theta, \theta))$. This, in turn, implies that

$$\begin{aligned} \mathbb{E}_{f \sim \mathcal{GP}(m_n, k_n)} [(**)^2] &\leq \exp(2m_n(\theta) + 2k_n(\theta, \theta)) + \exp(2g(\theta)) \\ &\leq \underbrace{\sup_{\theta \in \Theta} \exp(m_n(\theta) + k_n(\theta, \theta))^2 + \sup_{\theta \in \Theta} \exp(g(\theta))^2}_{=:C}. \end{aligned} \quad (5)$$

Combining the bounds (4) and (5), we have the overall bound of the original term $(*)$:

$$(*) \leq C \int_{\Theta} \mathbb{E}_{f \sim \mathcal{GP}(m_n, k_n)} [|f(\theta) - g(\theta)|^2] d\theta = C \mathbb{E}_{f \sim \mathcal{GP}(m_n, k_n)} \left[\int_{\Theta} |f(\theta) - g(\theta)|^2 d\theta \right]$$

where the order the integral and expectation can be interchanged by Fubini-Tonelli theorem, whenever the right-hand side is finite. Finally, it is straightforward to see from the definition of C that we have $C < 1$ if $m_n(\theta) + k_n(\theta, \theta) < (1/2) \log(1/2)$ and $g(\theta) < (1/2) \log(1/2)$. This concludes the proof because $-1/2 < \log(\sqrt{1/2})$ which is immediate to verify. \square

B.2 Proof of Theorem 1

We introduce two technical lemmas that will be useful. The first lemma is on a decomposition of the MMD. Recall that δ_N denotes the empirical distribution of the weighted samples $\{w_n^*, \theta_n^*\}_{n=1}^N$, and $d(p, \delta_N)$ denotes the MMD between the target density p and the empirical distribution δ_N .

Lemma 4. *Suppose that the target density $p(\cdot) = q(\cdot)/Z$ and the proposal density u are positive and continuous in Algorithm 1. Given an arbitrary proposal sequence $\{\theta_n\}_{n=1}^{M+N}$, define a functional*

$$I_{M+N}(f) := \left| \int_{\Theta} f(\theta) \frac{q(\theta)}{u(\theta)} u(\theta) d\theta - \frac{1}{N+M} \sum_{n=1}^{N+M} f(\theta_n) \frac{q(\theta_n)}{u(\theta_n)} \right|$$

for functions f on Θ . Then the weighted samples $\{w_n^*, \theta_n^*\}$ of Algorithm 1 satisfies

$$d(p, \delta_N) \leq B_1 \sup_{\|f\|_{\mathcal{H}_k} \leq 1} I_{M+N}(f) + B_2 I_{M+N}(1) + B_3 \frac{M}{N+M}$$

for some constants $B_1, B_2, B_3 > 0$ dependent only on p and u .

Proof. Recall that the target density $p(\theta)$ is defined as $p(\theta) = q(\theta)/Z$. Using the proposal density $u(\theta)$, we rewrite the MMD of interest $d(p, \delta_N)$ as follows:

$$d(p, \delta_N) = \sup_{\|f\|_{\mathcal{H}_\kappa} \leq 1} \left| \underbrace{\frac{1}{Z} \int_{\Theta} f(\theta) \frac{q(\theta)}{u(\theta)} u(\theta) d\theta - \sum_{i=1}^N w_n^* f(\theta_n^*)}_{=:(*)} \right| \quad \text{where} \quad w_n^* = \frac{\frac{1}{N} \frac{q(\theta_n^*)}{u(\theta_n^*)}}{\frac{1}{N} \sum_{n=1}^N \frac{q(\theta_n^*)}{u(\theta_n^*)}}.$$

For better presentation, define a function $h_f(\theta) := f(\theta)q(\theta)/u(\theta)$ for each f to see that

$$(*) = \left| \frac{\int_{\Theta} h_f(\theta) u(\theta) d\theta}{Z} - \frac{\frac{1}{N} \sum_{n=1}^N h_f(\theta_n^*)}{\frac{1}{N} \sum_{n=1}^N \frac{q(\theta_n^*)}{u(\theta_n^*)}} \right|$$

In addition, define two constants Z_{M+N} and Z_N^* by, respectively,

$$Z_{M+N} := \frac{1}{N+M} \sum_{n=1}^{M+N} \frac{q(\theta_n)}{u(\theta_n)} \quad \text{and} \quad Z_N^* := \frac{1}{N} \sum_{n=1}^N \frac{q(\theta_n^*)}{u(\theta_n^*)}.$$

By the triangle inequality, the term $(*)$ is upper-bounded as follows:

$$(*) \leq \underbrace{\left| \frac{\int_{\Theta} h_f(\theta) u(\theta) d\theta}{Z} - \frac{\frac{1}{N+M} \sum_{n=1}^{N+M} h_f(\theta_n)}{Z_{N+M}} \right|}_{=:(*)_1} + \underbrace{\left| \frac{\frac{1}{N+M} \sum_{n=1}^{N+M} h_f(\theta_n)}{Z_{N+M}} - \frac{\frac{1}{N} \sum_{n=1}^N h_f(\theta_n^*)}{Z_N^*} \right|}_{=:(*)_2}$$

where $\{\theta_n\}_{n=1}^{N+M}$ is the proposal sequence. For the term $(*)_1$, by the triangle inequality again,

$$(*)_1 \leq \underbrace{\left| \frac{\int_{\Theta} h_f(\theta) u(\theta) d\theta}{Z} - \frac{\frac{1}{N+M} \sum_{n=1}^{N+M} h_f(\theta_n)}{Z} \right|}_{=\frac{1}{Z} I_{M+N}(f)=:(*)_{11}} + \underbrace{\left| \frac{\frac{1}{N+M} \sum_{n=1}^{N+M} h_f(\theta_n)}{Z} - \frac{\frac{1}{N+M} \sum_{n=1}^{N+M} h_f(\theta_n)}{Z_{N+M}} \right|}_{=:(*)_{12}}.$$

We shall find a further upper bound of the latter term $(*)_{12}$. The term $(*)_{12}$ is upper bounded as

$$(*)_{12} = |Z - Z_{N+M}| \left| \frac{\frac{1}{N+M} \sum_{n=1}^{N+M} h_f(\theta_n)}{Z Z_{N+M}} \right| \leq \frac{1}{Z} |Z - Z_{N+M}| \underbrace{\frac{\frac{1}{N+M} \sum_{n=1}^{N+M} |h_f(\theta_n)|}{\frac{1}{N+M} \sum_{n=1}^{N+M} \frac{q(\theta_n)}{u(\theta_n)}}}_{=:(*)}.$$

Here, it follows from the definition of h_f and Lemma 1 that we have $|h_f(\theta)| \leq q(\theta)/u(\theta)$, where no absolute value is needed in the right-hand side since q and u are positive. This immediately implies that the term $(*)$ satisfies the upper bound $(*) \leq 1$. Therefore, we have

$$(*)_{12} \leq \frac{1}{Z} |Z - Z_{N+M}| = \frac{1}{Z} \left| \int_{\Theta} \frac{q(\theta)}{u(\theta)} u(\theta) d\theta - \frac{1}{N+M} \sum_{n=1}^{M+N} \frac{q(\theta_n)}{u(\theta_n)} \right| = \frac{1}{Z} I_{M+N}(1).$$

Finally, we shall find an upper bound of the term $(*_2)$. By the triangle inequality,

$$(*_2) \leq \underbrace{\left| \frac{\frac{1}{N+M} \sum_{n=1}^{N+M} h_f(\theta_n)}{Z_{N+M}} - \frac{\frac{1}{M+N} \sum_{n=1}^N h_f(\theta_n^*)}{Z_{N+M}} \right|}_{=:(*_21)} + \underbrace{\left| \frac{\frac{1}{M+N} \sum_{n=1}^N h_f(\theta_n^*)}{Z_{N+M}} - \frac{\frac{1}{N} \sum_{n=1}^N h_f(\theta_n^*)}{Z_N^*} \right|}_{=:(*_22)}.$$

Notice that, by construction, the proposal sequence $\{\theta_n\}_{n=1}^{M+N}$ can be disjointly decomposed into the samples $\{\theta_n^*\}_{n=1}^N$ obtained after the N -th iteration and the selection pool \mathcal{S}_{N+1} at the $(N+1)$ -th iteration. In other words, the proposal sequence $\{\theta_n\}_{n=1}^{M+N}$ is a union of the N samples $\{\theta_n^*\}_{n=1}^N$ and the selection pool \mathcal{S}_{N+1} at the $(N+1)$ -th iteration. Hence, the term $(*_21)$ can be expressed as

$$(*_21) = \left| \frac{\sum_{n=1}^{N+M} h_f(\theta_n) - \sum_{n=1}^N h_f(\theta_n^*)}{(M+N)Z_{M+N}} \right| = \left| \frac{\sum_{\theta \in \mathcal{S}_{N+1}} h_f(\theta)}{\sum_{n=1}^{M+N} q(\theta_n)/u(\theta_n)} \right| \leq \frac{\sum_{\theta \in \mathcal{S}_{N+1}} q(\theta)/u(\theta)}{\sum_{n=1}^{M+N} q(\theta_n)/u(\theta_n)}$$

where we used the fact that $|h_f(\theta)| \leq q(\theta)/u(\theta)$ again. Since q and u are both positive and continuous, the ratio $q(\cdot)/u(\cdot)$ is also positive and continuous. Since Θ is compact, the extreme value theorem implies that $q(\cdot)/u(\cdot)$ admits some maximum value U and minimum value L over Θ , where $U \geq L > 0$ due to the positivity. Notice also that, by construction, the selection pool \mathcal{S}_{N+1} always consists of M points across the iterations. These two facts provide an upper bound $\sum_{\theta \in \mathcal{S}_{N+1}} q(\theta)/u(\theta) \leq UM$ and a lower bound $\sum_{n=1}^{M+N} q(\theta_n)/u(\theta_n) \geq L(M+N)$. Therefore

$$(*_21) \leq \frac{U}{L} \frac{M}{M+N}.$$

We use the same argument for the term $(*_22)$. The term $(*_22)$ can be expressed as

$$\begin{aligned} (*_22) &= \left| \frac{\sum_{n=1}^N h_f(\theta_n^*)}{(M+N)Z_{N+M}} - \frac{\sum_{n=1}^N h_f(\theta_n^*)}{NZ_N^*} \right| \\ &= \frac{|(M+N)Z_{N+M} - NZ_N^*|}{(M+N)Z_{N+M}} \left| \frac{\sum_{n=1}^N h_f(\theta_n^*)}{NZ_N^*} \right| \\ &= \left| \frac{\sum_{n=1}^{M+N} q(\theta_n)/u(\theta_n) - \sum_{n=1}^N q(\theta_n^*)/u(\theta_n^*)}{\sum_{n=1}^{M+N} q(\theta_n)/u(\theta_n)} \right| \left| \frac{\sum_{n=1}^N h_f(\theta_n^*)}{\sum_{n=1}^N q(\theta_n^*)/u(\theta_n^*)} \right|. \end{aligned}$$

Since the proposal sequence $\{\theta_n\}_{n=1}^{M+N}$ can be disjointly decomposed into the samples $\{\theta_n^*\}_{n=1}^N$ and the selection pool \mathcal{S}_{N+1} , the same argument used for the term $(*_21)$ provides that

$$(*_22) \leq \frac{\sum_{\theta \in \mathcal{S}_{N+1}} q(\theta)/u(\theta)}{\sum_{n=1}^{M+N} q(\theta_n)/u(\theta_n)} \leq \frac{U}{L} \frac{M}{M+N}.$$

By all the arguments above, the MMD of interest $d(p, \delta_n)$ is bounded as

$$\begin{aligned} d(p, \delta_n) &\leq \sup_{\|f\|_{\mathcal{H}_K} \leq 1} (*_{11}) + \sup_{\|f\|_{\mathcal{H}_K} \leq 1} (*_{12}) + \sup_{\|f\|_{\mathcal{H}_K} \leq 1} (*_{21}) + \sup_{\|f\|_{\mathcal{H}_K} \leq 1} (*_{22}) \\ &\leq \frac{1}{Z} \sup_{\|f\|_{\mathcal{H}_K} \leq 1} I_{M+N}(f) + \frac{1}{Z} I_{M+N}(1) + 2 \frac{U}{L} \frac{M}{M+N}. \end{aligned}$$

Setting $B_1 = 1/Z$, $B_2 = 1/Z$, and $B_3 = 2U/L$ completes the proof. \square

The second technical lemma is an extension of the celebrated Koksma-Hlawka inequality to the domain Θ . Recall that D^* is the star discrepancy introduced in Section 4 and $\partial_{1:d}$ denotes the mixed partial derivative. Recall also the multi-index notation.

Lemma 5. *Let g be a function on Θ s.t. the first mixed partial derivative $\partial_{1:d}g(\theta)$ exists. Let $\{\theta_n\}_{n=1}^K$ be a sequence of K arbitrary points in Θ . We have*

$$\left| \int_{\Theta} g(\theta) d\theta - \frac{\text{Vol}(\Theta)}{K} \sum_{n=1}^K g(\theta_n) \right| \leq \text{Vol}(\Theta) V(g) D^*(\{\theta_n\}_{n=1}^K)$$

where $V(g)$ is the Hardy-Krause variation of the function g defined as follows:

$$V(g) := \sum_{\alpha \neq 0} \int_{\Theta^\alpha} |\partial^\alpha g(\theta_\alpha^*)| d\theta^\alpha$$

where $\alpha \neq 0$ is the binary multi-index α which is not zero vector $(0, \dots, 0)$.

Proof. Since Θ is hyperrectangular, Θ can be expressed as the product $[a_1, b_1] \times \dots \times [a_d, b_d]$ of some coordinatewise intervals $[a_i, b_i]$ for each $i = 1, \dots, d$. There exists a bijective affine map τ between the unit cube $[0, 1]^d$ and the domain Θ . Any point θ in Θ can be expressed as the image of some point η in $[0, 1]^d$ under the map τ . For each $i = 1, \dots, d$, let $\tau_i : [0, 1] \rightarrow [a_i, b_i]$ be a map s.t. $\theta_{(i)} = \tau_i(\eta_{(i)}) = a_i + (b_i - a_i)\eta_{(i)}$, where $\theta_{(i)}$ and $\eta_{(i)}$ denote the i -th coordinate of θ and η . Then, clearly, the bijective map τ is given by $\theta = \tau(\eta) = (\tau_1(\eta_{(1)}), \dots, \tau_d(\eta_{(d)}))$. Let $\{\eta_n\}_{n=1}^K$ be a sequence in $[0, 1]^d$ s.t. the image under the map τ corresponds to the original sequence $\{\theta_n\}_{n=1}^K$ in Θ . This means that $\theta_n = \tau(\eta_n)$ for each $n = 1, \dots, K$. By the change of variables, we have

$$\left| \int_{\Theta} g(\theta) d\theta - \frac{\text{Vol}(\Theta)}{K} \sum_{n=1}^K g(\theta_n) \right| = \text{Vol}(\Theta) \underbrace{\left| \int_{[0,1]^d} g \circ \tau(\eta) d\eta - \frac{1}{K} \sum_{n=1}^K g \circ \tau(\eta_n) \right|}_{=:(*)}$$

where we used that $\prod_{i=1}^d |(\partial/\partial\eta_{(i)})\tau_i(\eta_{(i)})| = \prod_{i=1}^d |b_i - a_i| = \text{Vol}(\Theta)$ for the change of variables. Recall the star discrepancy D^\dagger for the unit cube $[0, 1]^d$ defined in (3) in Appendix A.2. It follows from the Koksma-Hlawka inequality (Dick and Pillichshammer, 2010, Proposition 2.18) that

$$(*) \leq V^\dagger(g \circ \tau) D^\dagger(\{\eta_n\}_{n=1}^K). \quad (6)$$

where $V^\dagger(g \circ \tau)$ is the Hardy-Krause variation of the function $g \circ \tau$ defined by

$$V^\dagger(g \circ \tau) := \sum_{\alpha \neq 0} \int_{[0,1]^\alpha} |\partial^\alpha g \circ \tau(\eta_1^\alpha)| d\eta^\alpha. \quad (7)$$

Here η_1^α denotes a d -dimensional vector whose i -th coordinate is equal to that of η if $\alpha_i = 1$ and otherwise is fixed to a constant 1. We shall show that $V^\dagger(g \circ \tau) = V(g)$. Let I_α be a set of indices i s.t. $\alpha_i = 1$, by which the mixed partial derivative ∂^α can be expressed as $\partial^\alpha = \prod_{i \in I_\alpha} \partial_i$. By the chain rule and by that the map $\tau(\eta) = (\tau_1(\eta_{(1)}), \dots, \tau_d(\eta_{(d)}))$ is coordinatewise, we have

$$\partial^\alpha g \circ \tau(\eta_1^\alpha) = \partial^\alpha g(\theta)|_{\theta=\tau(\eta_1^\alpha)} \left(\prod_{i \in I_\alpha} \partial_i \tau_i(\eta_{(i)}) \right) = \partial^\alpha g(\theta)|_{\theta=\tau(\eta_1^\alpha)} \cdot \text{Vol}(\Theta^\alpha) \quad (8)$$

where we used $\prod_{i \in I_\alpha} \partial_i \tau_i(\eta_{(i)}) = \prod_{i \in I_\alpha} b_i - a_i = \text{Vol}(\Theta^\alpha)$. Denote by $h(\theta)$ the mixed partial derivative $\partial^\alpha g(\theta)$ to see that $h(\tau(\eta_1^\alpha)) = \partial^\alpha g(\theta)|_{\theta=\tau(\eta_1^\alpha)}$. Combining (7) and (8) gives that

$$V^\dagger(g \circ \tau) = \sum_{\alpha \neq 0} \int_{[0,1]^\alpha} \text{Vol}(\Theta^\alpha) |h(\tau(\eta_1^\alpha))| d\eta^\alpha.$$

Now recall that θ_*^α is a d -dimensional vector whose i -th coordinate is equal to that of θ if $\alpha_i = 1$ and otherwise is fixed to the constant b_i that is the right boundary of the hyperrectangular domain Θ at the i -th axis. We can express θ_*^α as $\theta_*^\alpha = \tau(\eta_1^\alpha)$ given that $\theta = \tau(\eta)$. We apply the change of variables to η^α to show that $V^\dagger(g \circ \tau) = V(g)$ as intended. Specifically, we apply the transform $\theta_{(i)} = \tau_i(\eta_{(i)})$ for each coordinate i s.t. $\alpha_i = 1$, to see that

$$V^\dagger(g \circ \tau) = \sum_{\alpha \neq 0} \int_{\Theta^\alpha} \text{Vol}(\Theta^\alpha) |h(\tau(\eta_1^\alpha))| d\eta^\alpha = \sum_{\alpha \neq 0} \int_{\Theta^\alpha} |\partial^\alpha g(\theta_*^\alpha)| d\theta^\alpha = V(g).$$

where $\text{Vol}(\Theta^\alpha)$ is cancelled by the change of variables. Therefore, the inequality (6) is rewritten as

$$(*) \leq V^*(g) D^\dagger(\{\eta_n\}_{n=1}^K)$$

By Lemma 3, we have $D^\dagger(\{\eta_n\}_{n=1}^K) = D^*(\{\theta_n\}_{n=1}^K)$, which concludes the proof. \square

Now we present the main proof:

Proof. First, we apply the upper bound of Lemma 4 to see that

$$d(p, \delta_N) \leq B_1 \underbrace{\sup_{\|f\|_{\mathcal{H}_k} \leq 1} I_{M+N}(f)}_{=:(*)_1} + B_2 \underbrace{I_{M+N}(1)}_{=:(*)_2} + B_3 \frac{M}{N+M}.$$

We shall upper bound the term $(*)_1$ and $(*)_2$ in what follows.

Upper Bounding $(*)_1$: Since u is uniform, the term $(*)_1$ can be bounded as follows:

$$(*)_1 = \sup_{\|f\|_{\mathcal{H}_\kappa} \leq 1} \left| \int_{\Theta} f(\theta) q(\theta) d\theta - \frac{\text{Vol}(\Theta)}{N+M} \sum_{n=1}^{N+M} f(\theta_n) q(\theta_n) \right| \leq \text{Vol}(\Theta) \underbrace{\sup_{\|f\|_{\mathcal{H}_\kappa} \leq 1} V(f \cdot q) D^*(\{\theta_n\}_{n=1}^{M+N})}_{=:(*)_{11}}$$

where the inequality follows from Lemma 5. We shall upper bound the term $(*)_{11}$, i.e., the supremum of the Hardy-Krause variation $V(f \cdot q)$. It is easy to see from the definition of V that

$$V(f \cdot q) \leq \sum_{\alpha \neq 0} \text{Vol}(\Theta^\alpha) \sup_{\theta \in \Theta^\alpha} |\partial^\alpha (f(\theta_*^\alpha) q(\theta_*^\alpha))| \leq \sum_{\alpha \neq 0} \text{Vol}(\Theta^\alpha) \underbrace{\sup_{\theta \in \Theta} |\partial^\alpha (f(\theta) q(\theta))|}_{=:(*)_{12}}.$$

Similarly to the product rule of derivatives, mixed partial derivatives can be extended by the general Leibniz rule. The general Leibniz rule slightly simplifies for binary multi-indices, in which case the mixed partial derivative of the product in the term $(*)_{12}$ can be expressed as follows:

$$\partial^\alpha (f(\theta) q(\theta)) = \sum_{\beta \leq \alpha} (\partial^{\alpha-\beta} f(\theta)) (\partial^\beta q(\theta))$$

where $\beta \leq \alpha$ means a binary multi-index β s.t. $\beta_i \leq \alpha_i$ for all $i = 1, \dots, d$. By Lemma 2, we have $\sup_{\theta \in \Theta} |\partial^{\alpha-\beta} f(\theta)| \leq 1$ for all $\alpha - \beta$ and all $\|f\|_{\mathcal{H}_\kappa} \leq 1$. By the assumption that $\partial_{1:d} q(\theta)$ is uniformly continuous, $\partial^\beta q(\theta)$ is uniformly continuous for any binary multi-index β . By the continuous extension theorem, $\partial^\beta q(\theta)$ can be continuously extended to the boundary of the domain Θ . This means that, by the extreme value theorem, there exists some constant C_q^β s.t. $\sup_{\theta \in \Theta} |\partial^\beta q(\theta)| \leq C_q^\beta$ for every binary multi-index β . By these two facts, we have

$$(*_{12}) \leq \sup_{\theta \in \Theta} \sum_{\beta \leq \alpha} \left| (\partial^{\alpha-\beta} f(\theta)) (\partial^\beta q(\theta)) \right| \leq \sum_{\beta \leq \alpha} C_q^\beta.$$

Since this bound of $(*_{12})$ holds for all $\|f\|_{\mathcal{H}_\kappa} \leq 1$, the original term $(*_{11})$ is bounded as

$$(*_{11}) \leq \sum_{\alpha \neq 0} \text{Vol}(\Theta^\alpha) \sum_{\beta \leq \alpha} C_q^\beta =: A_1$$

where we denote the constant in the right-hand side by A_1 .

Upper Bounding $(*_2)$: Since u is uniform, the term $(*_2)$ can be bounded as follows:

$$(*_2) = \left| \int_{\Theta} q(\theta) d\theta - \frac{\text{Vol}(\Theta)}{N+M} \sum_{n=1}^{N+M} q(\theta_n) \right| \leq \text{Vol}(\Theta) V(q) D^*(\{\theta_n\}_{n=1}^{M+N})$$

where the inequality follows from Lemma 5. It is easy to see from the definition of V that

$$V(q) \leq \sum_{\alpha \neq 0} \text{Vol}(\Theta^\alpha) \sup_{\theta \in \Theta^\alpha} |\partial^\alpha q(\theta)| \leq \sum_{\alpha \neq 0} \text{Vol}(\Theta^\alpha) \sup_{\theta \in \Theta} |\partial^\alpha q(\theta)|.$$

By the same argument as that used for upper-bounding the first term $(*_1)$, there exists some constant C_q^α s.t. $\sup_{\theta \in \Theta} |\partial^\alpha q(\theta)| \leq C_q^\alpha$ for every binary multi-index α . By this facts, we have

$$V(q) \leq \sum_{\alpha \neq 0} \text{Vol}(\Theta^\alpha) C_q^\alpha =: A_2$$

where we denote the constant in the right-hand side by A_2 .

Overall Bound: Plugging the derived upper bounds of $(*_1)$ and $(*_2)$ in, we have

$$(*) \leq \text{Vol}(\Theta) A_1 B_1 D^*(\{\theta_n\}_{n=1}^{M+N}) + \text{Vol}(\Theta) A_2 B_2 D^*(\{\theta_n\}_{n=1}^{M+N}) + B_3 \frac{M}{N+M}.$$

Setting $C_1 = \text{Vol}(\Theta) A_1 B_1 + \text{Vol}(\Theta) A_2 B_2$ and $C_2 = B_3$ concludes the proof. \square

B.3 Proof of Corollary 1

Proof. Recall that D^\dagger is the star discrepancy for the unit cube $[0, 1]^d$ defined in (3) in Appendix A.2. The scaled Halton sequence $\{\theta_i\}_{i=1}^\infty$ is defined as an image of the original Halton sequence $\{\eta_i\}_{i=1}^\infty$ under the bijective affine map. By Lemma 3, we have $D^*(\{\theta_n\}_{n=1}^K) = D^\dagger(\{\eta_n\}_{n=1}^K)$ for any number of points K . By Theorem 3.6 of Niederreiter (1992), there exists some constant $C > 0$ s.t. the star discrepancy D^\dagger of the original Halton sequence $\{\eta_n\}_{n=1}^K$ satisfies that

$$D^\dagger(\{\eta_n\}_{n=1}^K) \leq C \frac{\log(K)^d}{K}.$$

Combining this bound with the result of Theorem 1 concludes the proof. \square

B.4 Proof of Corollary 2

Proof. By assumption, the kernel κ is bounded, continuous, and integrally strictly positive definite. Hence, the resulting MMD metrises the weak convergence by Theorem 7 of Simon-Gabriel et al. (2023). By Corollary 1, the MMD between δ_N and p converges to zero, concluding the proof. \square

B.5 Proof of Theorem 2

The proof uses Lemma 4 presented in Appendix B.2, which holds for any proposal sequence.

Proof. First, we apply the upper bound of Lemma 4 to see

$$d(p, \delta_N) \leq B_1 \underbrace{\sup_{\|f\|_{\mathcal{H}_\kappa} \leq 1} I_{M+N}(f)}_{=:(*)_1} + B_2 \underbrace{I_{M+N}(1)}_{=:(*)_2} + B_3 \frac{M}{N+M}.$$

Define $g(\theta) := q(\theta)/u(\theta)$ to see that

$$I_{M+N}(f) = \left| \int_{\Theta} f(\theta) g(\theta) u(\theta) d\theta - \frac{1}{N+M} \sum_{n=1}^{N+M} f(\theta_n) g(\theta_n) \right|.$$

We shall upper bound the term $(*)_1$ and $(*)_2$ in what follows. Denote by u_{M+N} the empirical distribution of the proposal sequence $\{\theta_n\}_{n=1}^{M+N}$ for better presentation.

Upper Bounding $(*)_1$: Let \mathcal{H} be a set of functions s.t. $\mathcal{H} := \{f \mapsto f(\theta)g(\theta) \mid \|f\|_{\mathcal{H}_\kappa} \leq 1\}$ for the function g . Then, the term $(*)_1$ can be expressed as

$$(*)_1 = \sup_{\|f\|_{\mathcal{H}_\kappa} \leq 1} |\mathbb{E}_{\theta \sim u} [f(\theta)g(\theta)] - \mathbb{E}_{\theta \sim u_{M+N}} [f(\theta)g(\theta)]| = \sup_{h \in \mathcal{H}} |\mathbb{E}_{\theta \sim u} [h(\theta)] - \mathbb{E}_{\theta \sim u_{M+N}} [h(\theta)]|.$$

Recall that the proposal sequence $\{\theta_n\}_{n=1}^{M+N}$ is i.i.d. random samples from the proposal density u . Let $\{\epsilon_n\}_{n=1}^{M+N}$ be i.i.d. random variables taking the value in $\{+1, -1\}$ with equiprobability $1/2$. The Rademacher complexity $\mathcal{R}_{M+N}(\mathcal{H})$ of the set \mathcal{H} given the random variables $\{\theta_n\}_{n=1}^{M+N}$ is defined by

$$\begin{aligned} \mathcal{R}_{M+N}(\mathcal{H}) &:= \mathbb{E}_{\theta_1, \dots, \theta_{M+N}} \mathbb{E}_{\epsilon_1, \dots, \epsilon_{M+N}} \left[\sup_{h \in \mathcal{H}} \left| \frac{1}{M+N} \sum_{n=1}^{M+N} \epsilon_n h(\theta_n) \right| \right] \\ &= \mathbb{E}_{\theta_1, \dots, \theta_{M+N}} \mathbb{E}_{\epsilon_1, \dots, \epsilon_{M+N}} \left[\sup_{\|f\|_{\mathcal{H}_\kappa} \leq 1} \left| \frac{1}{M+N} \sum_{n=1}^{M+N} \epsilon_n f(\theta_n) g(\theta_n) \right| \right]. \end{aligned}$$

Lemma 1 implies that $|f(\theta)| \leq 1$ uniformly for all functions f s.t. $\|f\|_{\mathcal{H}_\kappa} \leq 1$. It is thus straightforward to see that any function $h \in \mathcal{H}$ is uniformly bounded by $b := \sup_{\theta \in \Theta} |g(\theta)|$ because

$$\sup_{\theta \in \Theta} |h(\theta)| \leq \sup_{\theta \in \Theta} |f(\theta)| \sup_{\theta \in \Theta} |g(\theta)| \leq \sup_{\theta \in \Theta} |g(\theta)| = b.$$

It then follows from Theorem 4.10 of Wainwright (2019) that

$$\mathbb{P}((*)_1 \leq 2\mathcal{R}_{M+N}(\mathcal{H}) + \delta) \geq 1 - \exp\left(-\frac{(M+N)\delta^2}{2b^2}\right) \quad (9)$$

where the probability \mathbb{P} is taken with respect to the i.i.d. random samples $\{\theta_n\}_{n=1}^{M+N}$. We shall upper bound the Rademacher complexity next. We apply the reproducing property of $f \in \mathcal{H}_\kappa$ to see

$$\begin{aligned}\mathcal{R}_{M+N}(\mathcal{H}) &= \mathbb{E}_{\theta_1, \dots, \theta_{M+N}} \mathbb{E}_{\epsilon_1, \dots, \epsilon_{M+N}} \left[\sup_{\|f\|_{\mathcal{H}_\kappa} \leq 1} \left| \frac{1}{M+N} \sum_{n=1}^{M+N} \epsilon_n \langle f(\cdot), \kappa(\cdot, \theta_n) \rangle_{\mathcal{H}_\kappa} g(\theta_n) \right| \right] \\ &= \frac{1}{M+N} \mathbb{E}_{\theta_1, \dots, \theta_{M+N}} \mathbb{E}_{\epsilon_1, \dots, \epsilon_{M+N}} \left[\sup_{\|f\|_{\mathcal{H}_\kappa} \leq 1} \left| \left\langle f(\cdot), \sum_{n=1}^{M+N} \epsilon_n \kappa(\cdot, \theta_n) g(\theta_n) \right\rangle_{\mathcal{H}_\kappa} \right| \right].\end{aligned}$$

We apply the fact that $\sup_{\|f\|_{\mathcal{H}_\kappa} \leq 1} |\langle f(\cdot), v(\theta) \rangle_{\mathcal{H}_\kappa}| = \|v(\theta)\|_{\mathcal{H}_\kappa}$ for any $v \in \mathcal{H}_\kappa$, which follows from the condition of the Cauchy-Schwartz inequality under which equality holds, to see that

$$\begin{aligned}\mathcal{R}_{M+N}(\mathcal{H}) &= \frac{1}{M+N} \mathbb{E}_{\theta_1, \dots, \theta_{M+N}} \mathbb{E}_{\epsilon_1, \dots, \epsilon_{M+N}} \left[\left\| \sum_{n=1}^{M+N} \epsilon_n \kappa(\cdot, \theta_n) g(\theta_n) \right\|_{\mathcal{H}_\kappa} \right] \\ &\leq \frac{1}{M+N} \sqrt{\mathbb{E}_{\theta_1, \dots, \theta_{M+N}} \mathbb{E}_{\epsilon_1, \dots, \epsilon_{M+N}} \left[\left\| \sum_{n=1}^{M+N} \epsilon_n \kappa(\cdot, \theta_n) g(\theta_n) \right\|_{\mathcal{H}_\kappa}^2 \right]} \\ &= \frac{1}{M+N} \sqrt{\mathbb{E}_{\theta_1, \dots, \theta_{M+N}} \mathbb{E}_{\epsilon_1, \dots, \epsilon_{M+N}} \left[\sum_{n=1}^{M+N} \sum_{m=1}^{M+N} \epsilon_n \epsilon_m g(\theta_n) \kappa(\theta_n, \theta_m) g(\theta_m) \right]}.\end{aligned}$$

In the above, the second inequality follows from the Jensen's inequality and the last equality follows from the reproducing property of the kernel κ . Note that the random variables ϵ_n and ϵ_m are independent when $n \neq m$, and that $\epsilon_n \epsilon_n = \epsilon_n^2 = 1$ with probability 1 by definition. Therefore

$$\begin{aligned}\mathcal{R}_{M+N}(\mathcal{H}) &\leq \frac{1}{M+N} \sqrt{\mathbb{E}_{\theta_1, \dots, \theta_{M+N}} \left[\sum_{n=1}^{M+N} g(\theta_n) \kappa(\theta_n, \theta_n) g(\theta_n) \right]} \\ &\leq \frac{1}{M+N} \sqrt{(M+N)b^2} \leq \frac{b}{\sqrt{M+N}}\end{aligned}$$

where the second inequality follows from that κ is bounded by 1 and that $g(\theta) \leq \sup_{\theta \in \Theta} |g(\theta)| = b$. Plugging this upper bound of $\mathcal{R}_{M+N}(\mathcal{H})$ in the concentration inequality (9) gives that

$$\mathbb{P} \left((*_1) \leq \frac{2b}{\sqrt{M+N}} + \delta \right) \geq 1 - \exp \left(-\frac{(M+N)\delta^2}{2b^2} \right) \geq 1 - 2 \exp \left(-\frac{(M+N)\delta^2}{2b^2} \right)$$

where the trivial inequality in the right-hand side is applied for convenience of subsequent analysis. This concentration inequality is equivalent to the following alternative expression

$$\mathbb{P} \left((*_1) \leq \frac{2b + \sqrt{2 \log(2/\epsilon)} b}{\sqrt{M+N}} \right) \geq 1 - \epsilon$$

where we set $\epsilon := 2 \exp(-(M+N)\delta^2/(2b^2)) > 0$.

Upper Bounding $(*_2)$: Define a function $F(\theta_1, \dots, \theta_{M+N}) := (1/(M+N)) \sum_{n=1}^{N+M} g(\theta_n)$. Since the proposal sequence $\{\theta_n\}_{n=1}^{M+N}$ is i.i.d. random variables, the term $(*_2)$ can be expressed as

$$(*_2) = |\mathbb{E}_{\theta \sim u} [g(\theta)] - \mathbb{E}_{\theta \sim u_{M+N}} [g(\theta)]| = \left| \mathbb{E}_{\theta_1, \dots, \theta_{M+N} \stackrel{i.i.d.}{\sim} u} [F(\theta_1, \dots, \theta_{M+N})] - F(\theta_1, \dots, \theta_{M+N}) \right|.$$

Our aim is to apply the bounded difference inequality in Corollary 2.21 of Wainwright (2019). The function F admits the ‘bounded difference’ with respect to each n -th argument θ_n . To see this, fix all arguments $\theta_1, \dots, \theta_{M+N}$, except the n -th argument θ_n , and observe for any n that

$$|F(\theta_1, \dots, \theta_n, \dots, \theta_{M+N}) - F(\theta_1, \dots, \theta'_n, \dots, \theta_{M+N})| = \frac{1}{M+N} |g(\theta_n) - g(\theta'_n)| \leq \frac{2b}{M+N}$$

where θ_n and θ'_n are arbitrary. Thus we can apply Corollary 2.21 of Wainwright (2019) to see that

$$\mathbb{P}((*_2) \leq \delta) \geq 1 - 2 \exp\left(-\frac{(M+N)\delta^2}{2b^2}\right)$$

where \mathbb{P} is the probability taken with respect to the i.i.d. random variables $\{\theta_n\}_{n=1}^{M+N}$. This concentration inequality is equivalent to the following alternative expression

$$\mathbb{P}\left((*_2) \leq \frac{\sqrt{2 \log(2/\epsilon)} b}{\sqrt{M+N}}\right) \geq 1 - \epsilon.$$

where we set $\epsilon := 2 \exp(-(M+N)\delta^2/(2b^2)) > 0$.

Overall Bound: Combining the concentration inequalities of $(*_1)$ and $(*_2)$, we have

$$\mathbb{P}\left(d(p, \delta_N) \leq B_1 \frac{2b + \sqrt{2 \log(2/\epsilon)} b}{\sqrt{M+N}} + B_2 \frac{\sqrt{2 \log(2/\epsilon)} b}{\sqrt{M+N}} + B_3 \frac{M}{N+M}\right) \geq 1 - \epsilon$$

Setting $C_1 = 2bB_1$, $C_2 = 2\sqrt{2}b$, and $C_3 = B_3$ concludes the proof. \square

B.6 Proof of Corollary 3

Proof. As shown in the proof of Corollary 2, the MMD of the kernel κ metrises the weak convergence. With no loss of generality, suppose that ϵ is small enough that $\sqrt{\log(2/\epsilon)} > 1$. Let C be a constant larger than C_1 , C_2 , and C_3M . Since $N \geq 1$ and $M \geq 1$, we have

$$d(p, \delta_N) \leq \frac{C_1 + C_2 \sqrt{\log(2/\epsilon)}}{\sqrt{N+M}} + C_3 \frac{M}{N+M} \leq \frac{C \sqrt{\log(2/\epsilon)}}{\sqrt{N+M}} =: \delta$$

Thus we have a simplified concentration inequality $\mathbb{P}(d(p, \delta_N) \leq \delta) \geq 1 - \epsilon$, which is equivalent to $\mathbb{P}(d(p, \delta_N) > \delta) \leq \epsilon$. This concentration inequality can be expressed in terms of δ as follows:

$$\mathbb{P}(d(p, \delta_N) > \delta) \leq 2 \exp\left(-\frac{\delta^2}{2C^2}(N+M)\right).$$

It then follows from the Borel-Cantelli lemma that $d(p, \delta_N)$ converges to zero almost surely in the limit $N \rightarrow 0$, meaning that δ_N weakly converges to p almost surely. \square

C Simulation Studies

This section presents additional simulation studies on BIS. Appendix C.1 discusses the importance of the point-selection procedure of BIS in comparison with the randomised BO. Appendix C.2 demonstrates the performance of BIS for different choices of the function ϕ . Appendix C.3 illustrates the performance of BIS for different choices of the size of the proposal sequence M .

C.1 Importance of Discrete Optimisation with No Revisit

In BO, the point at each iteration is selected by the optimisation over an infinite set, such as a compact subset of \mathbb{R}^d . In contrast, BIS select the point by the optimisation over a discrete set under the constraint that points selected in the past will never be revisited. The optimisation on the discrete set, together with the constraint, assists in efficient exploration of the domain of interest. It prevents cases where the point to be selected next will be arbitrarily close to the points already selected in the past. In the long run, therefore, the points selected in BIS do not concentrate on a particular subset of the domain. This is vital for the convergence guarantee of the importance sampling scheme.

The randomisation approach proposed in Kim and Sanz-Alonso (2024) extends BO with the aims of approximating posterior densities. They proposed performing BO while adding an extra random point in the training dataset of GP at each iteration. This means that at each iteration it obtains two points, where one of them is the point acquired by BO and the other is a random point. They showed the convergence of the GP posterior mean to a target posterior, when the GP is well specified. However, we shall demonstrate that importance sampling based on the points selected by such a randomised BO fails to recover the target posterior.

Figure 7 visualises 100 points obtained by the randomised BO of Kim and Sanz-Alonso (2024), for each benchmark density in Section 5.1. At each iteration of the randomised BO, a point from the scaled Halton sequence is used as the random point to add. Following the experimental setting in Section 5.1, the first 10 points were randomly selected from the Halton sequence. It illustrates that the points selected by BO (triangular) gradually concentrate to the maxima of the posterior density, while the random points from the Halton sequence (square) are dispersed over the domain. Figure 8 further confirms that importance sampling based on these samples fails to converge to the target posterior. For each target density, the approximation error of the resulting weighted samples deteriorated after a certain number of iterations.

The failure in the convergence roots in that points selected by BO concentrates at the mode of the target posterior after some iterations. Thus, after some iterations, the majority of the samples used for importance sampling are enforced to have one particular value, which is the mode. Moreover, those majority points sharing the same value are assigned the highest importance weights, since the mode is the point where the posterior probability is maximal by definition. Therefore, the influence of those majority points concentrating at the mode will be dominant. Roughly speaking, this means that, after some iterations, the weighted samples in the randomised BO starts approximating the Dirac distribution at the mode rather than the target density. On the other hand, BIS, by design, prevents such a concentration of samples.

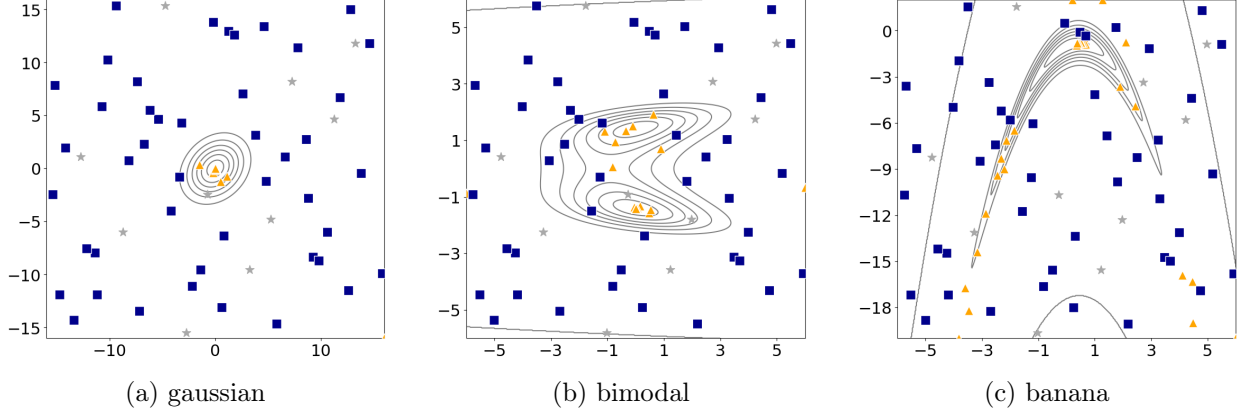


Figure 7: Visualisation of 100 samples obtained by the randomised BO of Kim and Sanz-Alonso (2024) for each benchmark density. The initial 10 points are star-shaped. The following points obtained by BO and QMC are illustrated in, respectively, triangle- and square-shaped. The contour values of each density were powered to $1/3$ for better visualisation of the tail geometry.

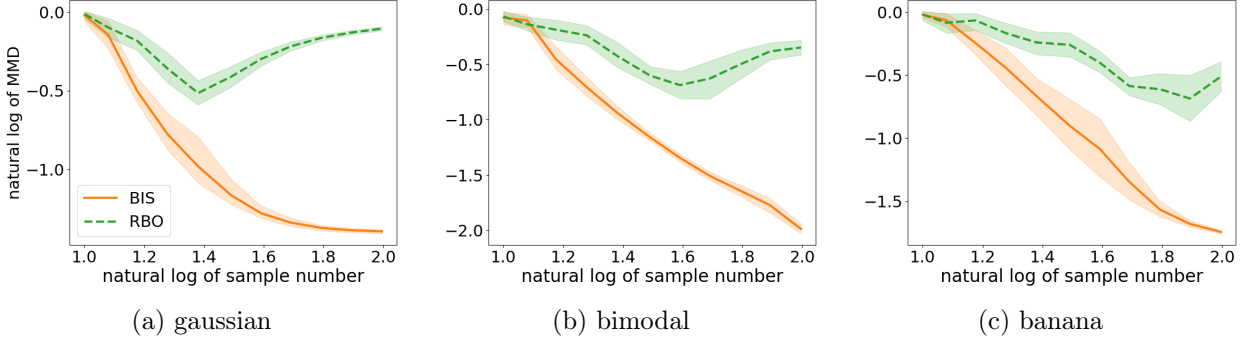


Figure 8: The approximation error of BIS (solid line) and standard importance sampling based on the points of the randomised BO (dashed line). The experiment was repeated 10 times, where the bold line represents the averaged error and the band represents the 95% confidence interval.

C.2 Different Choices of Function ϕ in GP-UJB

In Section 3.4, Table 1 listed examples of the function ϕ used in GP-UJB. This subsection compares the performance of BIS for different choices of the function ϕ through a simulation study. We used the experimental setting in Section 5.1, while changing the choice of the function ϕ . Figure 9 visualises 100 samples of BIS obtained for the banana density in Section 5.1, under three different choices of the function ϕ . It demonstrates that, under the quadratic function $\phi(x) = x^2$ and the relu function $\phi(x) = \max(x, 0)$, a relatively large portion of samples were situated outside the high probability region of the target density. On the other hand, the exponential function $\phi(x) = \exp(x)$ efficiently situated the majority of samples around the high probability region.

Figure 10 shows the approximation error of BIS for each benchmark density in Section 5.1, under three different choices of the function ϕ . While all three choices of the function ϕ provide a reasonable approximation error, the default choice $\phi(x) = \exp(x)$ achieved a relatively better approximation error overall. The approximation errors for the Gaussian and bimodal densities were

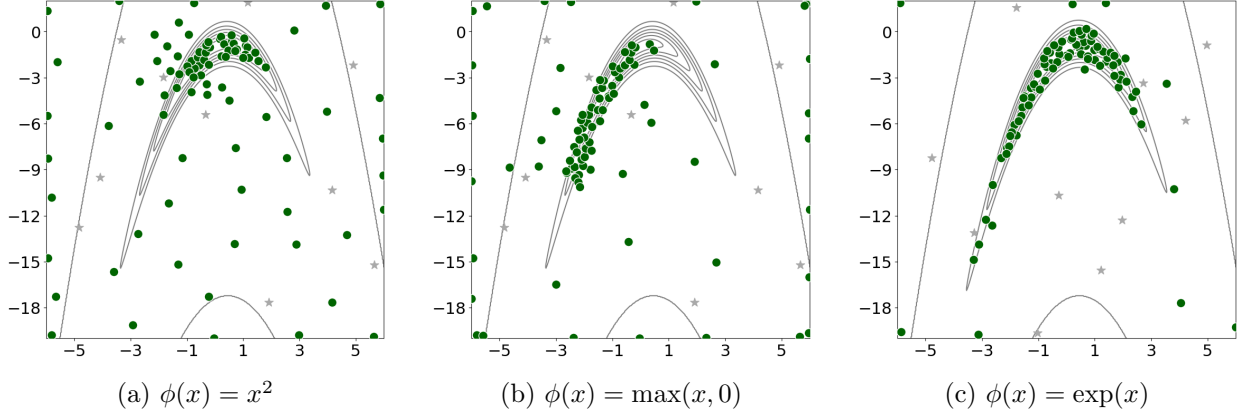


Figure 9: Visualisation of 100 samples of the banana density obtained by BIS for different ϕ . The contour values of the density were powered to $1/3$ for better visualisation of the tail geometry.

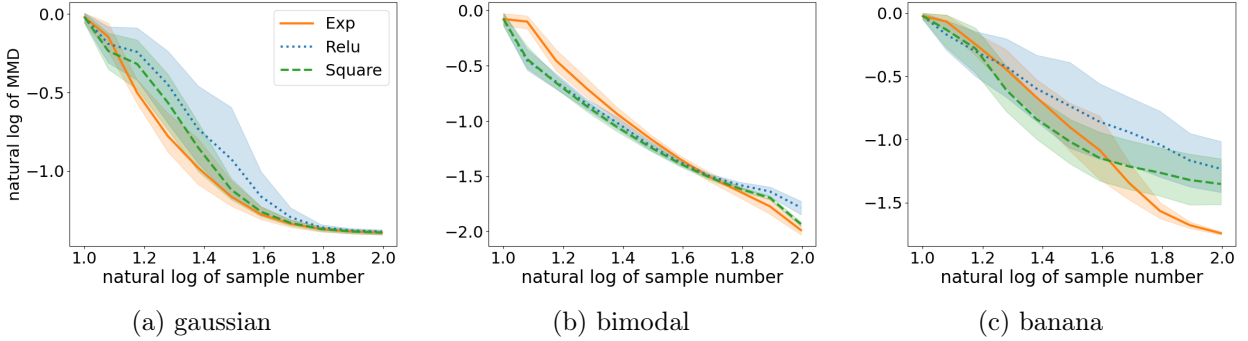


Figure 10: The approximation error of BIS for each benchmark density when the function $\phi(x)$ in GP-UJB is quadratic x^2 (dashed line), relu $\max(x, 0)$ (dotted line), and exponential $\exp(x)$ (solid line). The experiment was repeated 10 times, where the bold line represents the averaged error and the band represents the 95% confidence interval.

similar, and those for the banana density exhibit a difference, as also exemplified in Figure 9. Given this simulation study, we recommend the exponential function $\phi(x) = \exp(x)$ as the default choice to use in GP-UJB.

C.3 Sensitivity of Proposal-Sequence Size M

The size of the proposal sequence M is a hyperparameter of BIS. The convergence rates in Section 4 imply the trade-off between small and large values of the size M . If the size M is large, the first term in the convergence rates—regardless of the deterministic or probabilistic one—is suppressed, while the second term amplifies. Conversely, if the size M is small, the first term is not suppressed, while the second term does not amplify. In the extreme case where M is equal to one, BIS is identical to standard self-normalised importance sampling by construction. Choosing a reasonable value of the size M controls the trade-off, leading to an efficient approximation performance of BIS.

This subsection performs a simulation study on sensitivity of BIS to the size of the proposal sequence M . We used the experimental setting in Section 5.1, while changing the size of the

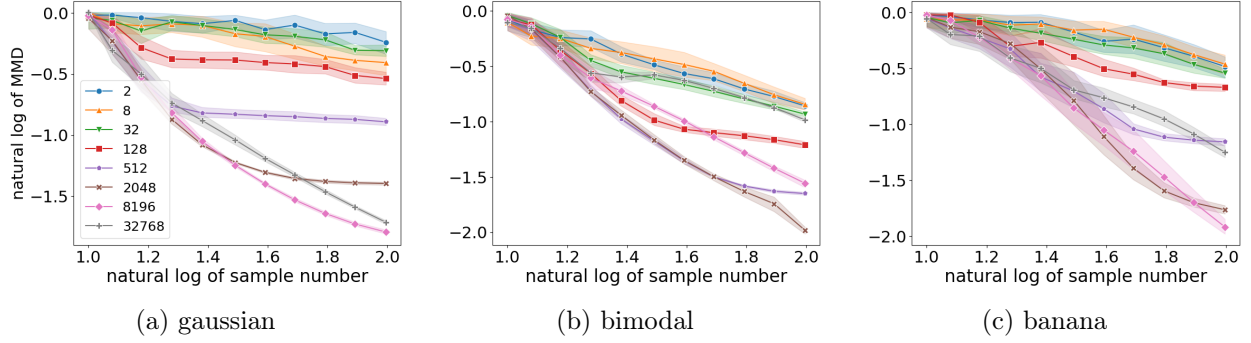


Figure 11: The approximation error of BIS for each benchmark density when the size of the proposal sequence is 2, 8, 32, 128, 512, 2048, 8196, and 32768. The experiment was repeated 10 times, where the bold line represents the averaged error and the band represents the 95% confidence interval.

proposal sequence M . Figure 11 shows the approximation error of BIS for each benchmark density, under different values of the proposal-sequence size M . As anticipated, when the size M was the small value 2, 8, and 32, the approximation performance of BIS got similar to that of standard importance sampling based on the scaled Halton sequence. In addition, the excessively large value of the proposal-sequence size $M = 32768$ didn't result in the best approximation performance of BIS. Overall, the size $M = 2048$ and $M = 8196$ led to the fastest decay of the approximation error of BIS. As the smaller size M reduces the computation cost in BIS, we recommend the size $M = 2048$ for experiments in two-dimensional domains based on this simulation study.

D Additional Experimental Details

This section provides additional details of the experiments presented in the main text. Appendix D.1 contains that of Section 5.1 and Appendix D.2 contains that of Section 5.2.

D.1 Additional Details of Section 5.1

All the benchmark densities are given in the form proposed in Järvenpää et al. (2021) s.t.

$$p(\theta) \propto \exp \left(-\frac{1}{2} \begin{bmatrix} T_1(\theta) \\ T_2(\theta) \end{bmatrix}^T \begin{bmatrix} 1 & \rho \\ \rho & 1 \end{bmatrix} \begin{bmatrix} T_1(\theta) \\ T_2(\theta) \end{bmatrix} \right).$$

Denote the first and second coordinates of the parameter θ by, respectively, θ_1 and θ_2 . The first unimodal Gaussian density is defined by $T_1(\theta) = \theta_1$, $T_2(\theta) = \theta_2$, and $\rho = 0.25$. The second bimodal density is defined by $T_1(\theta) = \theta_1$, $T_2(\theta) = \theta_2^2 - 2$, and $\rho = 0.5$. The third banana-shaped density is defined by $T_1(\theta) = \theta_1$, $T_2(\theta) = \theta_2 + \theta_1^2 + 1$, and $\rho = 0.9$. We used the Gaussian kernel for the covariance kernel k of the GP prior in GP-UJB. The explicit form is given by

$$k(\theta, \theta') = \sigma^2 \exp \left(-\frac{\|\theta - \theta'\|^2}{2l^2} \right)$$

where l is the length-scale constant and σ is the variance constant.

The approximation quality of the weighted samples of BIS was measured by MMD. The form (1) of MMD introduced in Section 4 admits a computationally-convenient alternative expression

$$\text{MMD}(p, q)^2 = \mathbb{E}_{\theta, \theta' \sim p}[\kappa(\theta, \theta')] - 2\mathbb{E}_{\theta \sim p, \theta' \sim q}[\kappa(\theta, \theta')] + \mathbb{E}_{\theta, \theta' \sim q}[\kappa(\theta, \theta')].$$

This alternative form of MMD can be efficiently estimated by Monte Carlo integration using samples from the densities p and q . Throughout the experiments, we used MMD associated with the Gaussian kernel $\kappa(\theta, \theta') = \exp(-0.5\|\theta - \theta'\|^2/h)$ with the constant $h = 0.1$.

The approximation quality of the GP surrogate density was measured by TVD. The explicit form of TVD between two densities p and q is given as follows:

$$\text{TVD}(p, q) := \frac{1}{2} \int_{\Theta} |p(\theta) - q(\theta)| d\theta.$$

We approximate the integral over Θ by numerical integration. In this experiment, the densities p and q to be plugged in TVD are available only up to the normalising constants. We also approximate their normalising constants by numerical integration. Let $\{\eta_i\}_{i=1}^N$ be the N points from the scaled Halton sequence on the domain Θ . Denote the volume of the domain Θ by V . Let \tilde{p} and \tilde{q} be the proportional terms of the densities p and q . Then their normalising constants, denoted by Z_p and Z_q , are approximated as follows:

$$Z_p \approx \frac{V}{N} \sum_{i=1}^N \tilde{p}(\eta_i) =: \hat{Z}_p \quad \text{and} \quad Z_q \approx \frac{V}{N} \sum_{i=1}^N \tilde{q}(\eta_i) =: \hat{Z}_q.$$

Finally, TVD between the densities p and q is numerically computed by

$$\text{TVD}(p, q) \approx \frac{V}{2N} \sum_{i=1}^N \left| \frac{\tilde{p}(\eta_i)}{\hat{Z}_p} - \frac{\tilde{q}(\eta_i)}{\hat{Z}_q} \right|.$$

We used the $N = 10,000$ points from the scaled Halton sequence throughout.

Table 2 summarised the number of samples required for standard importance sampling to surpass the approximation error of 100 weighed samples obtained by BIS. For standard importance sampling, we used the scaled Halton sequence as samples and assigned self-normalised importance weights to them. It demonstrates that standard importance sampling required nearly 2,000 samples on average to achieve the approximation error that BIS does with 100 samples.

Table 2: The number of samples required for standard importance sampling to surpass the approximation error of 100 BIS weighed samples. The experiment was repeated 10 times, where the averaged number was reported together with the standard deviation in a bracket.

target density	number of samples	approximation error
gaussian	2368 (\pm 232)	0.040 (\pm 0.002)
bimodal	1324 (\pm 223)	0.010 (\pm 0.002)
banana	2487 (\pm 293)	0.018 (\pm 0.001)

D.2 Additional Details of Section 5.2

The synthetic likelihood of the modified Lorentz weather model is computed using summary statistics of sample paths simulated from the model. Denote by $s \in \mathbb{R}^d$ summary statistics of the observed sample path, for some dimension d . Denote by $s(\theta) \in \mathbb{R}^d$ summary statistics of a sample path simulated from the model under a parameter θ , where $s(\theta)$ is a random variable induced by simulation from the model. Let $m(\theta) \in \mathbb{R}^d$ and $\Sigma(\theta) \in \mathbb{R}^{d \times d}$ be the mean and covariance of $s(\theta)$. The synthetic likelihood at θ is then the Gaussian density $N(s \mid m(\theta), \Sigma(\theta))$ evaluated at the summary statistics s of data. In practice, the mean and covariance are estimated from multiple i.i.d. realisations of the summary statistics $s(\theta)$. Thus, the synthetic likelihood is computed using multiple sample paths simulated from the model at each θ . For the modified Lorentz weather model, Hakkarainen et al. (2012) used the following six summary statistics: (i) mean of $x_k(t)$ over time, (ii) variance of $x_k(t)$ over time, (iii) autocovariance of $x_k(t)$ with time lag one, (iv) covariance of $x_k(t)$ and $x_{k+1}(t)$ over time, (v) cross covariance of $x_k(t)$ and $x_{k-1}(t)$ with time lag one, (vi) cross covariance of $x_k(t)$ and $x_{k+1}(t)$ with time lag one. The summary statistics computed for each variable $x_k(t)$ is averaged over k . Thus, we have six-dimensional summary statistics for each sample path of the 40 variables.